

Locally Private Online Quantile Regression: Estimation and Inference

Yi Liu* and Qirui Hu^{†‡}

Abstract

We study estimation and inference for online quantile regression under a one-report user-level ε -locally differentially private (ε -LDP) protocol. The main difficulty is that the standard quantile-regression estimating-equation couples covariates with a residual comparison, so a server that receives only privatized reports cannot form the usual online update. We address this by developing a finite-alphabet channel in which each user computes the contribution locally, applies support-aware stochastic quantization and randomized response to one selected-block category, and sends one report. A public decoder corrects the randomized-response distortion and reconstructs a server-side estimating-equation input with the correct conditional mean. These decoded inputs are then used in projected Polyak-Ruppert averaging. For fixed finite channel designs, we establish local privacy, decoder unbiasedness, consistency, asymptotic normality, and Hessian-free self-normalized inference for prespecified scalar contrasts. Simulations and a New York City taxi-trip illustration show that the private trajectory approaches the nonprivate online reference as the privacy budget grows and outperforms direct Laplace and face-exponential geometric releases in the reported regimes.

Keywords: finite-alphabet LDP mechanisms, local differential privacy, online quantile regression, self-normalized inference, stochastic approximation

*York University

[†]Shanghai University of Finance and Economics

[‡]Corresponding author: huqirui@mail.shufe.edu.cn

1 Introduction

Quantile regression (QR) estimates conditional quantiles, or their linear-projection analogues under possible misspecification, by minimizing the asymmetric check loss of Koenker and Bassett [1978]; see also Koenker [2005], Angrist et al. [2006]. It is useful when conditional means give an incomplete distributional summary, for example under skewness, tail heterogeneity, or quantile-specific covariate effects. In modern data streams with sensitive records, the privacy risk is not limited to transmitting (X, Y) : deterministic functions of a participant’s record can also reveal sensitive attributes or participation. This motivates randomizing participant-side information before any server-side computation.

Local differential privacy (LDP) formalizes this trust model. Unlike central differential privacy, where a trusted curator first observes the database and then releases a privatized output [Dwork et al., 2006], LDP requires each user to randomize the record before transmission [Warner, 1965, Duchi et al., 2013, 2018]. Thus the server observes only a randomized report whose distribution is stable, up to the factor e^ϵ , under changes to the participant’s contribution. We study fixed-dimensional linear QR with bounded covariates under a one-record, one-report user-level ϵ -LDP protocol; Definition 1 gives the formal privacy condition. The server may broadcast any public or predictable query information, including the current online iterate and a public quantization design.

This setting creates an obstruction that is absent from ordinary online QR. Mathematically, at quantile level τ , a standard online update is driven by the estimating-equation contribution

$$g_\beta(X, Y) = X \{ \mathbf{1}(Y \leq X^\top \beta) - \tau \}.$$

The server needs both the covariate vector and the residual comparison $\mathbf{1}(Y \leq X^\top \beta)$ to form this vector, but under user-level ϵ -LDP it observes neither directly. Thus the problem is not simply to perturb an available stochastic gradient: the privatized report must protect the participant’s contribution while its decoded version retains the conditional mean structure required by stochastic approximation.

Existing methods cover adjacent settings but not this one-report locally private estimating-equation problem. Nonprivate online QR assumes an observable record-level update [Shen et al., 2025a]; scalar locally private quantile methods do not involve covariate-dependent regression updates [Liu et al., 2023, 2024, Cai et al., 2025, Amand et al., 2025, Cai et al., 2026b, Hu and Liu, 2026]; and central or distributed private QR relies on different trust or aggregation models [Chen and Chua, 2023, Tran et al., 2024, Shen et al., 2025b, Lu et al., 2026]. We therefore formulate locally private online QR as a decoded estimating-equation problem in which LDP reports satisfy user-level ϵ -LDP and decoded server inputs preserve the mean needed for averaged stochastic approximation. Three questions guide the development.

First, can a single data-dependent LDP report be decoded into an unbiased QR estimating-equation input at every public iterate?

Second, how does the finite randomized-response alphabet affect the effective information available to the online recursion?

Third, can confidence statements be built from the decoded private trajectory without estimating the QR Hessian?

To answer these questions, we construct a support-aware finite-alphabet channel for decoded estimating equations. At each iterate, the user computes $g_\beta(X, Y)$ locally. The QR residual comparison places this vector on one of two support faces, and bounded covariates restrict selected coordinates to public intervals. The user stochastically quantizes selected coordinates on a public grid, applies randomized response to the resulting finite category, and sends only the LDP report. The server applies an affine randomized-response decoder and Horvitz-Thompson coordinate reconstruction. Writing \tilde{g}_β for the decoded server-side input, the key property is conditional unbiasedness:

$$\mathbb{E} \{ \tilde{g}_\beta(X, Y) \mid X, Y, \beta \} = g_\beta(X, Y).$$

Privacy is a property of the LDP report received by the server; estimation and inference are post-processing operations applied to the decoded trajectory.

The paper makes the following contributions.

1. We formulate streaming linear QR under a sequential one-report user-level ε -LDP protocol as a decoded estimating-equation problem, separating the privacy guarantee for the report from the conditional-mean requirement for stochastic approximation.
2. We construct the $\text{CQ}_X(q, s)$ channel, where q is the slope-coordinate grid size and s is the selected block size. The channel combines public coordinate selection, support-aware stochastic quantization, randomized response, affine decoding, and Horvitz-Thompson reconstruction using the two-face support geometry of the QR estimating-equation contribution.
3. We prove local privacy and conditional decoder unbiasedness for the exact QR estimating-equation contribution. For fixed finite channel designs, we establish consistency and asymptotic normality of the projected Polyak-Ruppert averaged estimator under fixed-dimensional regularity conditions, with limiting covariance reflecting both sampling variation and privacy-channel randomization.
4. We provide Hessian-free inference based on the decoded private trajectory, including a self-normalized confidence procedure for prespecified scalar contrasts and divide-and-conquer and HiGrad-style studentization procedures with explicit rank and calibration conditions.

5. We empirically assess privacy-accuracy-inference tradeoffs through simulations across privacy budgets, dimensions, quantile levels, and inferential targets, together with a New York City taxi-trip illustration, benchmarking the proposed channel against direct Laplace and face-exponential geometric releases and nonprivate online stochastic approximation.

We next review related work and compare the proposed framework with adjacent method classes.

Online and communication-constrained quantile regression. Classical QR models distributional features beyond the mean [Koenker and Bassett, 1978, Koenker, 2005], including projection interpretations under misspecification [Angrist et al., 2006]. Recent online QR work studies stochastic subgradient methods when records arrive sequentially and the update is directly observable [Shen et al., 2025a]. Distributed and communication-constrained QR addresses data split across machines or institutions with controlled communication [Tan et al., 2022]. Our focus is instead the sequential one-report LDP setting, where each record is privatized before the server forms a decoded estimating-equation input by post-processing an LDP report.

Local privacy mechanisms and private regression. The LDP literature studies the statistical cost of replacing raw records by local randomized reports [Duchi et al., 2013, 2018]. Randomized response, RAPPOR, extremal mechanisms, subset selection, Hadamard response, and related finite-channel methods provide mechanism tools for categorical and distributional tasks [Warner, 1965, Erlingsson et al., 2014, Kairouz et al., 2016, Ye and Barg, 2018, Acharya et al., 2019, Pastore and Gastpar, 2021]. A separate line studies non-interactive LDP empirical risk minimization and regression, including generalized linear models and structural assumptions that reduce sample complexity [Wang et al., 2020, 2023].

Generic numeric-vector LDP methods can be applied to an estimating-equation vector [Wang et al., 2019, Li et al., 2020, Asi et al., 2022, 2023], but they treat the contribution as an ambient numeric object. Our construction instead uses the QR two-face support geometry and decodes a categorical privatized report to recover the estimating-equation contribution in conditional mean.

Private quantiles and private QR inference. Private quantile estimation has a longer central-DP literature. Smooth-sensitivity and robust-statistical constructions give early DP mechanisms for medians and related quantile-type statistics [Nissim et al., 2007, Dwork and Lei, 2009, Smith, 2011]. Recent work studies exact or approximate multiple quantiles, private quantile functions, bounded-space streaming quantiles, and high or unbounded quantiles [Gillenwater et al., 2021, Kaplan et al., 2022, Lalanne et al., 2023, Alabi et al., 2023, Durfee, 2023, Imola et al., 2025]. Under local privacy, scalar quantile and CDF procedures provide inference for one-dimensional distributional targets using binary queries, adaptive protocols, or histogram/range-query primitives [Liu et al., 2023, 2024, Cai et al., 2025, Aamand et al., 2025, Gaboardi et al., 2019, Cormode et al., 2019, Bassily and Smith, 2015, Canonne and Gentle, 2025]. These methods do not require covariate-dependent QR updates.

Related one-bit quasi-MLE and federated quantile-inference methods study complementary local or distributed protocols [Ono et al., 2022, Cai et al., 2026a]. Central and distributed DP QR methods protect

estimators or optimization procedures under curator or server-side models [Chen and Chua, 2023, Tran et al., 2024, Shen et al., 2025b, Lu et al., 2026], while central-DP quantile algorithms address scalar or multiple quantile release [Gillenwater et al., 2021, Kaplan et al., 2022, Durfee, 2023]. This differs from the one-report local model considered here.

Inference for stochastic approximation and private outputs. Our estimation theory uses Polyak-Ruppert averaging and standard martingale tools for stochastic approximation [Ruppert, 1988, Polyak and Juditsky, 1992, Robbins and Siegmund, 1971, Kushner and Yin, 2003, Hall and Heyde, 1980, Bach and Moulines, 2011]. For uncertainty quantification, self-normalization, batch means, online bootstrap, divide-and-conquer ideas, and HiGrad-style hierarchical grouping are closely related [Shao, 2010, Chen et al., 2020, Zhu and Dong, 2021, Fang et al., 2018, Banerjee et al., 2019, Su and Zhu, 2023]. Differentially private inference methods emphasize that valid confidence statements must account for the privatized output, not only the sampling distribution of the nonprivate estimator [Dette and Graw, 2024, Xie et al., 2025, Wang et al., 2025]. Here, the privacy channel enters both the covariance and the finite-sample stability of confidence procedures.

Table 1 compares the proposed setting with adjacent method classes. To our knowledge, this is the first one-report LDP framework for online QR estimation and inference based on mean-preserving decoded estimating-equation inputs rather than direct additive-noise SGD.

The remainder is organized as follows. Section 2 presents the target, sequential LDP model, decoded estimating-equation framework, support geometry, and channel. Section 3 gives estimation and inference theory; Sections 4 and 5 report simulations and the taxi illustration; Section 6 concludes. Appendices A and B report simulation implementation details and additional numerical summaries; proofs are deferred to the supplementary proof document.

2 Methodology and Local Privacy Mechanism

2.1 Preliminaries

Let $W_i \in [-1, 1]^p$ denote the bounded non-intercept covariate vector and set $X_i = (1, W_i^\top)^\top \in \mathbb{R}^{p+1}$. The private record is $\mathcal{O}_i = (W_i, Y_i)$, equivalently (X_i, Y_i) after appending the deterministic intercept. The observations are i.i.d. copies of $\mathcal{O} = (X, Y)$, and the coefficient vector $\beta \in \mathbb{R}^{p+1}$ includes the intercept. For a fixed quantile level $\tau \in (0, 1)$, write

$$\rho_\tau(u) = u \{\tau - \mathbf{1}(u < 0)\}.$$

The target parameter is

$$\beta^* = \arg \min_{\beta \in \mathcal{B}} M(\beta), \quad M(\beta) = \mathbb{E} \{ \rho_\tau(Y - X^\top \beta) \}, \quad (1)$$

Table 1: Comparison with adjacent private quantile, quantile-regression, and local-privacy methods. A \checkmark means that representative work in the method class directly addresses the requirement; a \times means that the requirement is outside that line’s stated target, trust model, timing model, or inferential output.

Requirement	Scalar LDP Q/CDF	CDP Q	Shuf./ dist. Q	Online QR	Dist. QR	DP QR	LDP ERM / GLM	Online private SGD	This paper
Record randomized before server analysis	\checkmark	\times	\checkmark	\times	\times	\times	\checkmark	\checkmark	\checkmark
One data-dependent report per participant	\checkmark	\times	\checkmark	\times	\times	\times	\checkmark	\checkmark	\checkmark
Online stochastic update path	\checkmark	\times	\times	\checkmark	\times	\times	\times	\checkmark	\checkmark
Regression covariates	\times	\times	\times	\checkmark	\checkmark	\checkmark	\checkmark	\checkmark	\checkmark
Quantile-regression coefficient target	\times	\times	\times	\checkmark	\checkmark	\checkmark	\times	\times	\checkmark
CI or confidence-set inference	\checkmark	\times	\times	\times	\checkmark	\checkmark	\checkmark	\checkmark	\checkmark
Server update uses only LDP reports	\checkmark	\times	\checkmark	\times	\times	\times	\checkmark	\checkmark	\checkmark

Representative work. Scalar LDP Q/CDF includes Liu et al. [2023, 2024], Cai et al. [2025], Aamand et al. [2025]. Central-DP (CDP) scalar or multiple quantile release includes Nissim et al. [2007], Dwork and Lei [2009], Gillenwater et al. [2021], Kaplan et al. [2022], Lalanne et al. [2023], Alabi et al. [2023], Durfee [2023], Imola et al. [2025]; these papers use a trusted-curator model and do not provide locally randomized QR updates. Shuffle or distributed private quantile protocols include Aamand et al. [2025]. Online QR is represented by Shen et al. [2025a], and distributed QR by Tan et al. [2022]. Central or distributed DP QR includes Chen and Chua [2023], Tran et al. [2024], Shen et al. [2025b], Lu et al. [2026], Wang et al. [2025]. LDP ERM/GLM includes Wang et al. [2020, 2023], Ono et al. [2022], Wang et al. [2019], Li et al. [2020], Asi et al. [2022, 2023]. Online private SGD inference includes Xie et al. [2025], Dette and Graw [2024]. A checkmark for a method class means that representative work in the class has the row feature; it does not mean every cited paper in the class has that feature.

where $\mathcal{B} \subset \mathbb{R}^{p+1}$ is compact and convex. The regularity conditions in Section 3 require uniqueness of this minimizer and the local density and nonsingularity assumptions needed for asymptotic linearization. Define

$$m(\beta) = \mathbb{E}\{g_\beta(\mathcal{O})\}, \quad g_\beta(\mathcal{O}) = X\{\mathbf{1}(Y \leq X^\top \beta) - \tau\}.$$

We refer to $g_\beta(\mathcal{O})$ as the exact QR estimating-equation contribution. Under local privacy this vector may be computed on the user side, but it is never transmitted to the server. When $Y | X$ has a conditional density at $X^\top \beta^*$, the Jacobian of m at the target, under the above sign convention, is

$$H = \mathbb{E}\{f_{Y|X}(X^\top \beta^* | X) X X^\top\}. \tag{2}$$

The matrix H is the QR Hessian appearing in the asymptotic variance. The inference procedures considered later avoid estimating H directly.

Definition 1 (Sequential one-report local differential privacy). *Let Q_i collect all public information fixed before user i 's record is randomized, including the current iterate, selected coordinate block, grid, privacy budget, relabeling rule, and any external randomness used by the server. A sequentially queried one-report protocol is ε -locally differentially private (ε -LDP) for the participant's one-record contribution $\mathcal{O}_i = (W_i, Y_i)$ if, conditional on every possible value of Q_i , for all measurable output sets \mathcal{U} and all record pairs o, o' ,*

$$\mathbb{P}\{\mathcal{M}_i(o) \in \mathcal{U} \mid Q_i\} \leq e^\varepsilon \mathbb{P}\{\mathcal{M}_i(o') \in \mathcal{U} \mid Q_i\}.$$

This is the standard conditional formulation for LDP protocols with public or predictable sequential queries [Duchi et al., 2013, Dwork and Roth, 2014]. The budget ε is per user: all design choices may depend on past LDP reports and external randomness, but must be fixed before the current record is randomized, while decoding, reconstruction, averaging, comparisons, and confidence sets are post-processing. The one-report constraint matches streaming settings in which each record is available once.

Definition 2 (Decoded estimating-equation channel). *Fix a public query point $\beta \in \mathcal{B}$, a public channel specification θ , a local randomization rule $\mathcal{M}_{\theta, \beta}$, a public decoder $D_{\theta, \beta}$, and a record $o = (x, y)$. Let*

$$\tilde{Z} = \mathcal{M}_{\theta, \beta}(o), \quad \tilde{g}_\theta(\beta) = D_{\theta, \beta}(\tilde{Z}),$$

where \tilde{Z} is the LDP report. The pair $(\mathcal{M}_{\theta, \beta}, D_{\theta, \beta})$ is an unbiased ε -LDP decoded estimating-equation channel if \tilde{Z} is ε -LDP for the participant's one-record contribution and

$$\mathbb{E}\{\tilde{g}_\theta(\beta) \mid \mathcal{O} = o, \beta, \theta\} = g_\beta(o).$$

For coordinate-block channels, this full-vector unbiasedness averages over the record-independent block draw. Let B be the realized public block, P_B the coordinate projection, $\pi_j = \Pr(j \in B)$ the public coordinate inclusion probability, and D_B^{blk} the selected-block decoder. The block decoder satisfies

$$\mathbb{E}\left\{D_B^{\text{blk}}(\tilde{Z}) \mid \mathcal{O} = o, \beta, B\right\} = P_B g_\beta(o).$$

The full vector is then formed by Horvitz-Thompson reconstruction and by averaging over the data-independent block draw:

$$\mathbb{E}\{\tilde{g}_\theta(\beta) \mid \mathcal{O} = o, \beta\} = g_\beta(o).$$

Conditioning additionally on a realized block gives coordinate mean $\mathbf{1}(j \in B) g_{\beta, j}(o) / \pi_j$; the full-vector equality above averages over the public block randomization.

The online recursion uses the decoded input, not the LDP report. The query β_{i-1} is determined by the server state before the current public block is drawn. Section 3 gives the pre-block/post-block conditioning distinction; the full mean field is recovered only after averaging over the fresh record-independent block. With $\Pi_{\mathcal{B}}$ denoting Euclidean projection onto \mathcal{B} , the projected stochastic-approximation update is

$$\beta_i = \Pi_{\mathcal{B}} \{ \beta_{i-1} - \eta_i \tilde{g}_i(\beta_{i-1}) \}, \quad \eta_i = \eta_0 i^{-\gamma}, \quad \gamma \in (1/2, 1).$$

The decoded sequence has the form $\tilde{g}_1(\beta_0), \tilde{g}_2(\beta_1), \dots, \tilde{g}_n(\beta_{n-1})$, and the reported estimator is the Polyak average

$$\bar{\beta}_n = n^{-1} \sum_{i=1}^n \beta_i. \quad (3)$$

At a fixed β , the privacy-channel noise is $\tilde{g}_\theta(\beta) - g_\beta(\mathcal{O})$, whereas the martingale estimating-equation noise in the stochastic-approximation analysis is $\tilde{g}_\theta(\beta) - m(\beta)$. At β^* , where $m(\beta^*) = 0$,

$$\tilde{g}_\theta(\beta^*) = g_{\beta^*}(\mathcal{O}) + \{ \tilde{g}_\theta(\beta^*) - g_{\beta^*}(\mathcal{O}) \},$$

so the decoded input contains both the ordinary QR estimating-equation fluctuation and the additional channel noise induced by local randomization.

The finite-alphabet channel below exploits the exact support of a single-record QR contribution. For $x = (1, z^\top)^\top$ with $z \in [-1, 1]^p$, define

$$S_\beta(o) = \mathbf{1}(y \leq x^\top \beta) - \tau \in \{-\tau, 1 - \tau\}.$$

Then

$$g_\beta(o) = x S_\beta(o), \quad g_{\beta,0}(o) = S_\beta(o), \quad g_{\beta,j}(o) = S_\beta(o) z_j, \quad j = 1, \dots, p.$$

Thus the exact support of $g_\beta(o)$ is

$$\mathcal{G}_\tau = \{-\tau\} \times [-\tau, \tau]^p \cup \{1 - \tau\} \times [-(1 - \tau), 1 - \tau]^p,$$

with ℓ_1 -diameter

$$\Delta_1 = \sup_{u,v \in \mathcal{G}_\tau} \|u - v\|_1 = \max\{p + 1, 2p \max(\tau, 1 - \tau)\}. \quad (4)$$

The intercept coordinate identifies the active face. Conditional on this face, each slope coordinate lies in a symmetric interval with radius

$$|S_\beta(o)| = \begin{cases} \tau, & S_\beta(o) = -\tau, \\ 1 - \tau, & S_\beta(o) = 1 - \tau. \end{cases}$$

Let $r_{\max} = \max\{\tau, 1 - \tau\}$. If the face coordinate is available, selected slopes can be encoded on the covariate scale because $g_j/g_0 = z_j \in [-1, 1]$; otherwise the channel uses the unconditional estimating-equation interval $[-r_{\max}, r_{\max}]$.

This geometry explains why several natural private releases are not well matched to online QR. Scalar LDP quantile protocols protect one-dimensional threshold information, but the QR update requires the product of a residual comparison and the covariate vector. Separately releasing covariates and residual signs would require multiple LDP reports or a product-category construction, without using the two-face support or directly providing the decoded full-vector contribution used by the online recursion. Generic numeric-vector LDP mechanisms can be applied to $g_\beta(\mathcal{O})$, but treat the update as an ambient vector. The two geometric baselines below isolate the resulting tradeoff: direct Laplace release preserves the mean but ignores support, whereas a face-restricted exponential release preserves support but generally shifts the mean.

A direct Laplace estimating-equation release sends

$$Z^{\text{Lap}} = g_\beta(\mathcal{O}) + \ell^{\text{Lap}}, \quad \ell_j^{\text{Lap}} \stackrel{\text{iid}}{\sim} \text{Laplace}(\Delta_1/\varepsilon), \quad j = 0, \dots, p. \quad (5)$$

Because $\|g_\beta(o) - g_\beta(o')\|_1 \leq \Delta_1$ for all records o, o' , the release in (5) is ε -LDP. It is unbiased under the identity decoder, but its output lies in \mathbb{R}^{p+1} , not in \mathcal{G}_τ , so privacy noise is spent in infeasible QR directions. Each coordinate receives privacy-noise variance $2(\Delta_1/\varepsilon)^2$, a cost especially visible when $p+1$ is moderate or ε is small because the ℓ_1 -diameter in (4) governs all coordinates simultaneously.

A support-preserving face-exponential mechanism draws $Z^{\text{EM}} \in \mathcal{G}_\tau$ from

$$\Pr(Z^{\text{EM}} \in dv \mid g_\beta(\mathcal{O})) \propto \exp\left\{-\frac{\varepsilon}{2\Delta_1} \|v - g_\beta(\mathcal{O})\|_1\right\} \mu_\tau(dv), \quad v \in \mathcal{G}_\tau, \quad (6)$$

where μ_τ is the sum of the p -dimensional Lebesgue measures on the two faces, with counting measure in the degenerate case $p = 0$. The utility sensitivity is at most Δ_1 , so (6) is ε -LDP. However, the conditional mean of Z^{EM} generally differs from $g_\beta(\mathcal{O})$, because the density is truncated on the two faces and also mixes between them. If this release is inserted directly into stochastic approximation, the recursion follows a perturbed mean field rather than $m(\beta)$. Thus support preservation alone is not enough for QR estimation; the server-side update must also be correct in conditional mean.

These alternatives isolate the two failures that the proposed channel avoids. Separate private releases of covariates and residual signs do not directly produce the coupled QR contribution and would require multiple reports or a larger product category. Direct Laplace release preserves the estimating-equation mean but spends privacy noise outside the QR support, whereas the face-exponential release preserves the two-face support but generally shifts the conditional mean and hence the stochastic-approximation target. The coordinate-quantized channel instead privatizes one selected-block finite category and applies an affine randomized-response inverse, so the decoded server-side input is mean preserving after Horvitz-Thompson reconstruction, even though the final decoded vector need not lie in \mathcal{G}_τ . Section 4 gives numerical evidence that the proposed LDP mechanism outperforms these two designs in the reported regimes for estimation error and uncertainty quantification.

Figure 1 illustrates the two-face QR support for $p = 0, 1, 2$ and $\tau = 0.5, 0.75$, together with the two geometric baselines used in the numerical study. A direct Laplace release preserves the estimating-equation mean by adding centered ambient noise but ignores the feasible set. A face-exponential release remains on the feasible support but generally does not preserve the conditional mean. The coordinate-quantized channel instead privatizes a support-aware finite category for the selected block and applies a public affine inverse, yielding a decoded update with the correct conditional mean even though the final decoded vector is not constrained to lie in \mathcal{G}_τ .

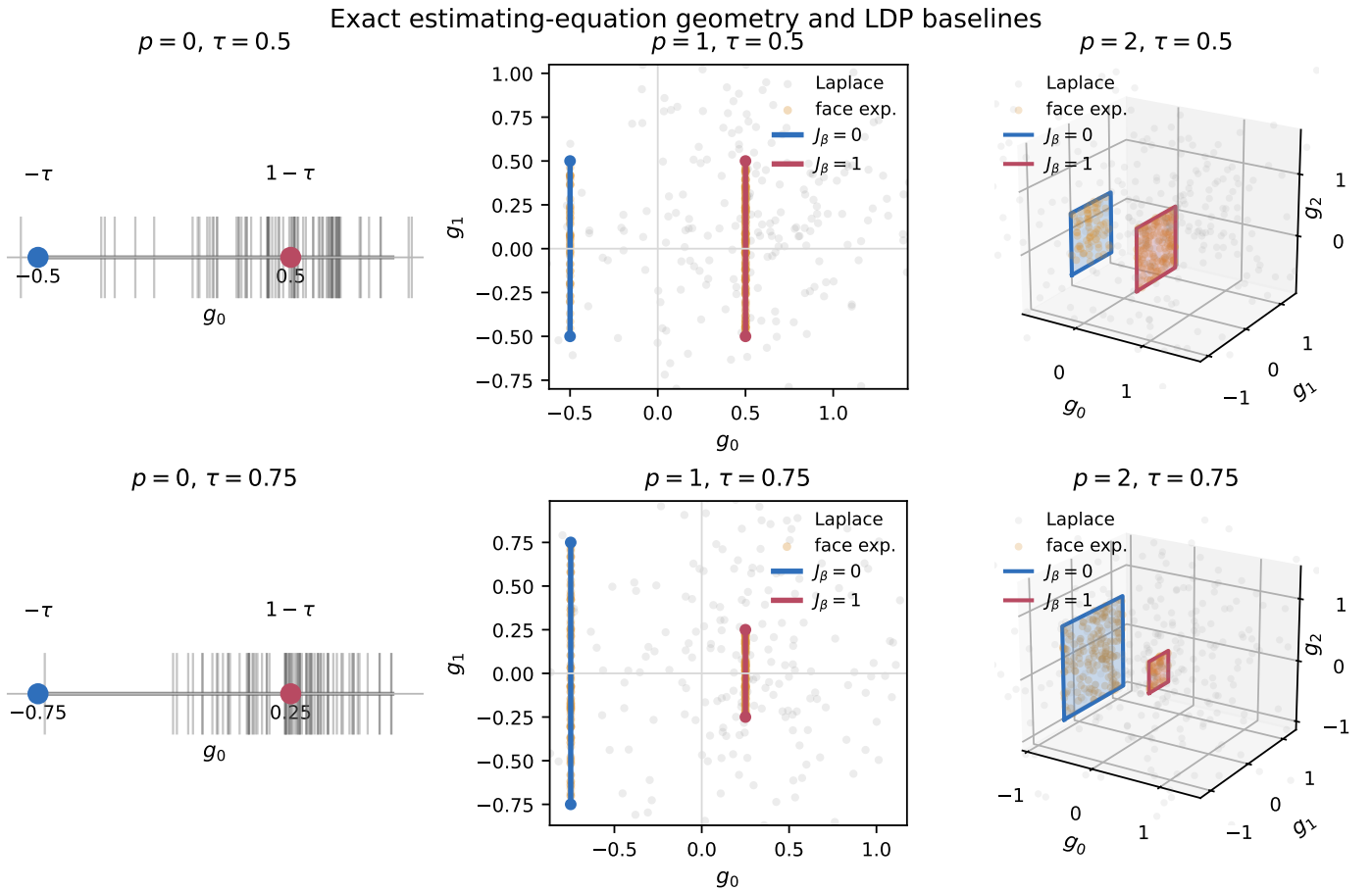


Figure 1: Feasible exact local QR estimating-equation contributions and geometric baseline LDP releases for $p = 0, 1, 2$. Here $J_\beta = \mathbf{1}(Y \leq X^\top \beta)$, so $J_\beta = 0$ and $J_\beta = 1$ are the two faces. Blue and red objects show the exact support. Gray marks show direct-Laplace releases: vertical ticks on the g_0 axis for $p = 0$, and points in the displayed estimating-equation coordinates for $p \geq 1$. Orange marks show face-exponential releases for $p \geq 1$. The panels illustrate why support awareness must be paired with mean-preserving decoding.

2.2 Coordinate-Quantized Mechanism $\text{CQ}_X(q, s)$

We now specify the channel $\text{CQ}_X(q, s)$. Estimating-equation coordinates are indexed by $0, 1, \dots, p$, with coordinate 0 the intercept and active face, and coordinates $1, \dots, p$ the slopes associated with W . The integer $q \in \{2, 3, \dots\}$ is the number of slope-grid levels, and $s \in \{1, \dots, p+1\}$ is the number of selected estimating-equation coordinates in one report. Let $B \subset \{0, \dots, p\}$ be the public selected block, with $|B| = s$. The finite- q channel is used for estimation and inference; $q = \infty$ is reserved for nonprivate limiting references below.

The selected block is sampled uniformly without replacement from the $p+1$ estimating-equation coordinates and is independent of the current record. Therefore

$$\pi_j = \Pr(j \in B) = \frac{s}{p+1}, \quad j = 0, \dots, p.$$

For $p = 0$, the selected block is necessarily $B = \{0\}$ and $\pi_0 = 1$. The Horvitz-Thompson factor $1/\pi_j$ is applied only to selected coordinates; unselected coordinates are filled with zero.

Fix a realized block B and write $g = g_\beta(o)$. Stochastic rounding first maps the selected coordinates to a finite latent category without introducing discretization bias. If $0 \in B$, the intercept coordinate is the two-point face variable $g_0 \in \{-\tau, 1 - \tau\}$. For each selected slope coordinate $j \in B \setminus \{0\}$, define $u_j = g_j/g_0 = z_j \in [-1, 1]$, which is well defined because $\tau \in (0, 1)$. Let

$$\mathcal{A}_q = \left\{ -1 + \frac{2\ell}{q-1} : \ell = 0, \dots, q-1 \right\}.$$

Adjacent-grid stochastic rounding produces $\zeta_j \in \mathcal{A}_q$ with $\mathbb{E}(\zeta_j | g_j, g_0) = u_j$. The selected-block representative uses $g_0\zeta_j$ on the estimating-equation scale and is therefore unbiased for g_j .

If $0 \notin B$, the report contains no face label. Each selected slope coordinate is rounded directly on the public grid

$$\mathcal{A}_q(r_{\max}) = \left\{ -r_{\max} + \frac{2r_{\max}\ell}{q-1} : \ell = 0, \dots, q-1 \right\},$$

again using adjacent-grid stochastic rounding with conditional mean equal to the exact selected coordinate. In both cases, the quantization step produces a latent category Λ_B and a selected-block representative $v_B(\Lambda_B)$ satisfying

$$\mathbb{E}\{v_B(\Lambda_B) | g, B\} = P_B g. \quad (7)$$

The entire privacy budget is spent on one categorical release for the selected block. Let $\iota_B = \mathbf{1}(0 \in B)$, $s_B^{\text{slope}} = |B| - \iota_B$ and the block alphabet size is $K_B = 2^{\iota_B} q^{s_B^{\text{slope}}}$. For this fixed block, write the latent category set as $\mathcal{K}_B = \{1, \dots, K_B\}$. The public map $v_B : \mathcal{K}_B \rightarrow \mathbb{R}^{|B|}$ assigns to each category its selected-block representative on the estimating-equation scale. The user never releases Λ_B or $v_B(\Lambda_B)$.

The privatized report is the randomized-response output index $\tilde{\Lambda}$:

$$\Pr(\tilde{\Lambda} = \lambda | \Lambda_B = \lambda) = \frac{e^\epsilon}{e^\epsilon + K_B - 1}, \quad \Pr(\tilde{\Lambda} = \lambda' | \Lambda_B = \lambda) = \frac{1}{e^\epsilon + K_B - 1}, \quad \lambda' \neq \lambda. \quad (8)$$

Define the randomized-response contraction factor

$$\kappa_{\text{rr}}(K_B, \varepsilon) = \frac{e^\varepsilon - 1}{e^\varepsilon + K_B - 1} \quad (9)$$

and the uniform selected-grid mean

$$\bar{v}_B = K_B^{-1} \sum_{\lambda \in \mathcal{K}_B} v_B(\lambda). \quad (10)$$

With the public relabeling suppressed in the notation,

$$\mathbb{E} \left\{ v_B(\tilde{\Lambda}) \mid \Lambda_B = \lambda, B \right\} = \bar{v}_B + \kappa_{\text{rr}}(K_B, \varepsilon) \{v_B(\lambda) - \bar{v}_B\}.$$

The affine block decoder inverts this contraction:

$$D_B^{\text{blk}}(\tilde{\Lambda}) = \bar{v}_B + \frac{v_B(\tilde{\Lambda}) - \bar{v}_B}{\kappa_{\text{rr}}(K_B, \varepsilon)}. \quad (11)$$

The full decoded estimating-equation vector is

$$\tilde{g}_j = \begin{cases} D_{B,j}^{\text{blk}}(\tilde{\Lambda}) / \pi_j, & j \in B, \\ 0, & j \notin B. \end{cases} \quad (12)$$

The decoded range may extend beyond the exact two-face support because the affine decoder corrects randomized-response shrinkage and the Horvitz-Thompson step inflates selected coordinates. This has no privacy consequence, since decoding and reconstruction are post-processing of the privatized report. It does affect the variance through K_B , $\kappa_{\text{rr}}(K_B, \varepsilon)$, and π_j . The full procedure is summarized in Algorithm 1.

Algorithm 1 Locally private online quantile-regression ASGD

1. Given $\tau, (q, s, \varepsilon), \mathcal{B}, \beta_0, \eta_i = \eta_0 i^{-\gamma}$ with $\gamma \in (1/2, 1)$, stream length n , and reporting set $\mathcal{T} \subset \{1, \dots, n\}$, set $\bar{\beta}_0 = \beta_0$.
2. For $i = 1, \dots, n$:
 - (a) Draw $B_i \subset \{0, \dots, p\}$ uniformly without replacement with $|B_i| = s$, independently of $\mathcal{O}_i = (X_i, Y_i)$, set $\pi_j = s / (p + 1)$, and send $(\beta_{i-1}, B_i, q, \varepsilon, \tau)$ and the public relabeling convention to user i .
 - (b) User i forms $g_i = g_{\beta_{i-1}}(\mathcal{O}_i)$ and applies the block rounding construction above to obtain Λ_{B_i} , so that (7) holds with $B = B_i$ and $g = g_i$.
 - (c) User i sends only the privatized report $\tilde{\Lambda}_i$, generated from Λ_{B_i} by the randomized-response law (8).
 - (d) The server evaluates $\kappa_{\text{rr}}(K_{B_i}, \varepsilon)$ from (9), \bar{v}_{B_i} from (10), decodes by (11), and forms $\tilde{g}_i(\beta_{i-1})$ by the reconstruction rule (12).
 - (e) Update

$$\beta_i = \Pi_{\mathcal{B}} \{ \beta_{i-1} - \eta_i \tilde{g}_i(\beta_{i-1}) \}, \quad \bar{\beta}_i = (i-1)i^{-1} \bar{\beta}_{i-1} + i^{-1} \beta_i.$$

Store $\bar{\beta}_i$ if $i \in \mathcal{T}$, and store trajectory values needed for post-processing inference.

3. Return $\bar{\beta}_n, \{\bar{\beta}_t : t \in \mathcal{T}\}$, and the stored decoded trajectory.
-

The next proposition collects the privacy, unbiasedness, finite-range, and local-stability properties of $\text{CQ}_X(q, s)$ used by the online analysis.

Proposition 1 (Privacy, unbiasedness, and finite range of $\text{CQ}_X(q, s)$). *For any finite $q < \infty$, any $1 \leq s \leq p + 1$, and any $\varepsilon > 0$, the channel $\text{CQ}_X(q, s)$ satisfies the following properties.*

1. *Conditional on the public selected block, the randomized-response output $\tilde{\Lambda}$ is ε -locally differentially private for the participant's one-record contribution. Mixing over data-independent selected blocks preserves the same guarantee.*

2. *The selected-block decoder and full Horvitz-Thompson reconstruction satisfy*

$$\mathbb{E} \left\{ D_B^{\text{blk}}(\tilde{\Lambda}) \mid g, B \right\} = P_B g, \quad \mathbb{E}(\tilde{g} \mid g) = g,$$

where the second expectation also averages over the data-independent public block draw.

3. *For every fixed finite design (q, s, ε) , the decoded vector is uniformly bounded over all records, query points, selected blocks, and possible randomized-response outputs:*

$$\sup_{\beta \in \mathcal{B}} \sup_{\circ} \sup_{\tilde{\Lambda}} \|\tilde{g}\|_2 \leq C_{\text{CQ}}(p, \tau, q, s, \varepsilon) < \infty.$$

4. *Under a common implementation of the public block draw, stochastic rounding, and randomized response, two decoded inputs queried at β and β' are identical for a fixed record whenever*

$$\mathbf{1}(y \leq x^\top \beta) = \mathbf{1}(y \leq x^\top \beta').$$

Hence local changes in the decoded input occur only on the usual QR slab between the two hyperplanes.

The parameters q , s , and ε control different parts of the privacy-accuracy tradeoff. The grid size q sets the resolution of the selected slope coordinates: larger q reduces stochastic-rounding variability but increases the alphabet size $K_B = 2^{\mathbf{1}(0 \in B)} q^{|B|-1(0 \in B)}$. For fixed ε , larger K_B decreases $\kappa_{\text{tr}}(K_B, \varepsilon)$ in (9), so the affine decoder amplifies centered randomized-response noise by $1/\kappa_{\text{tr}}(K_B, \varepsilon)$. Thus q is not monotone for accuracy at finite privacy budget: it trades quantization error against randomized-response inversion noise.

The block size s determines how many estimating-equation coordinates are queried in one local report. Larger s reduces Horvitz-Thompson inflation because $\pi_j = s/(p + 1)$ increases, and $s = p + 1$ removes coordinate subsampling. At the same time, larger s usually increases K_B , so it may increase randomized-response noise when ε is fixed. The design therefore spends the entire privacy budget on one selected-block category rather than splitting ε coordinate by coordinate.

The privacy budget ε acts only through the randomized-response channel. For fixed K_B ,

$$\kappa_{\text{tr}}(K_B, \varepsilon) \uparrow 1 \quad \text{as } \varepsilon \rightarrow \infty, \quad \kappa_{\text{tr}}(K_B, \varepsilon) \downarrow 0 \quad \text{as } \varepsilon \downarrow 0.$$

At small ε , $\kappa_{\text{rr}}(K_B, \varepsilon) \approx \varepsilon/K_B$, so affine decoding can greatly inflate server-side variance. At large ε , randomized-response noise vanishes, leaving only finite-grid and coordinate-subsampling losses.

Several special cases connect $\text{CQ}_X(q, s)$ to familiar procedures.

1. **Scalar quantile case.** If $p = 0$, then $B = \{0\}$, $K_B = 2$, and q is irrelevant. The mechanism reduces to binary randomized response applied to $S_\beta(Y) = \mathbf{1}(Y \leq \beta) - \tau$. The resulting recursion is the scalar online LDP quantile stochastic-approximation scheme, with affine decoding of the randomized binary response [Liu et al., 2023].
2. **Coarsest finite member.** When $q = 2$, adjacent-grid stochastic rounding reduces each selected slope to one of the two endpoints of its public interval. This is the coarsest stochastic-rounding member of the family, analogous to unbiased low-precision or quantized-gradient schemes [Gupta et al., 2015, Alistarh et al., 2017]. With $s = 1$, each user reports one randomized selected-coordinate category. It has low communication and small alphabet size, but it uses only one coordinate from each participant contribution and therefore relies heavily on Horvitz-Thompson reconstruction.
3. **All-coordinate finite-grid release.** When $s = p + 1$ and $q < \infty$, all estimating-equation coordinates are selected and $\pi_j = 1$. The channel becomes a finite-grid randomized-response release of the whole QR contribution. Since the intercept is always included, the selected slopes are quantized on the covariate scale and then mapped back to the estimating-equation scale.
4. **No randomized-response noise.** If $\varepsilon = \infty$ while $q < \infty$, then $\kappa_{\text{rr}}(K_B, \varepsilon) = 1$ and the randomized-response step becomes the identity. This regime corresponds to finite-precision stochastic approximation with quantized arithmetic or quantized gradients, as in practical low-precision CPU/GPU implementations and communication-efficient SGD [Gupta et al., 2015, Alistarh et al., 2017]. The procedure is no longer private, but finite stochastic quantization and, if $s < p + 1$, coordinate subsampling remain. The decoded input is still conditionally unbiased for $g_\beta(\mathcal{O})$.
5. **Private continuous-response releases.** If $q = \infty$ while $\varepsilon < \infty$, the finite-alphabet randomized-response construction is replaced by a continuous LDP release of the bounded estimating-equation contribution, for example through Laplace-type noise calibrated to the contribution’s public sensitivity. Such mechanisms are useful baselines, but they are outside the finite-channel theory developed here.
6. **Nonprivate online QR reference.** The simultaneous limit $q = \infty, s = p + 1, \varepsilon = \infty$ removes stochastic quantization, coordinate subsampling, and randomized-response noise. In this limit, $\tilde{g}_i(\beta_{i-1}) = g_{\beta_{i-1}}(\mathcal{O}_i)$, and the update reduces to the ordinary nonprivate projected averaged stochastic-approximation algorithm for QR, as in nonprivate online QR and Polyak-Ruppert averaging [Shen et al., 2025a, Ruppert, 1988, Polyak and Juditsky, 1992].

Thus $\text{CQ}_X(q, s)$ is a coordinate-quantized template for bounded estimating-equation contributions beyond QR; below we focus mainly on $q < \infty$ and $\varepsilon < \infty$.

3 Asymptotic Properties

3.1 Assumptions and Main Results

We now study the decoded online trajectory produced by the finite channel in Section 2. Recall that the privatized report of user i is denoted by \tilde{Z}_i ; for the channel $\text{CQ}_X(q, s)$, this is the randomized category $\tilde{\Lambda}_i$ in Algorithm 1. The decoded vector that the server would obtain at query point β is denoted by $\tilde{g}_i(\beta)$, and the actually observed decoded input is $\tilde{g}_i(\beta_{i-1})$.

Let \mathcal{P}_t collect the public server randomness at completed step t , including B_t and any public relabeling. Fixed design quantities are deterministic, or equivalently included in \mathcal{H}_0 . For the analysis, define the pre-block server history

$$\mathcal{H}_{i-1} = \sigma \left\{ \beta_0, \mathcal{P}_1, \tilde{Z}_1, \dots, \mathcal{P}_{i-1}, \tilde{Z}_{i-1} \right\}.$$

This analysis filtration is not an online-storage requirement: the implementation may keep only its recursive state S_{i-1} , such as β_{i-1} , $\bar{\beta}_{i-1}$, online normalizers, or trajectory summaries; this state is \mathcal{H}_{i-1} -measurable. The iterate, step size, grid, privacy budget, coordinate-selection law, and relabeling rules are also \mathcal{H}_{i-1} -measurable. The public block B_i is drawn after \mathcal{H}_{i-1} , independently of \mathcal{H}_{i-1} , the current record $\mathcal{O}_i = (X_i, Y_i)$, and the current local-randomizer auxiliary randomness. Write

$$\mathcal{F}_{i-1}^+ = \mathcal{H}_{i-1} \vee \sigma(B_i)$$

for the enlarged public state after the block draw. Conditional on \mathcal{F}_{i-1}^+ , the local randomizer $\mathcal{O}_i \mapsto \tilde{Z}_i$ is ε -LDP for the participant's one-record contribution. All decoded estimators, averages, normalizers, confidence intervals, and ellipsoids below are post-processing of the server-side transcript of LDP reports.

For stochastic approximation, martingale differences are conditioned on the pre-block history \mathcal{H}_{i-1} , not the enlarged post-block state \mathcal{F}_{i-1}^+ . Define the Horvitz-Thompson block operator

$$\{\mathcal{R}_B v\}_j = \frac{\mathbf{1}(j \in B)}{\pi_j} v_j, \quad j = 0, \dots, p.$$

For every \mathcal{H}_{i-1} -measurable query point β , the selected-block reconstruction has the conditional means

$$\mathbb{E} \{ \tilde{g}_i(\beta) \mid \mathcal{O}_i, \mathcal{F}_{i-1}^+ \} = \mathcal{R}_{B_i} g_\beta(\mathcal{O}_i), \quad \mathbb{E} \{ \tilde{g}_i(\beta) \mid \mathcal{F}_{i-1}^+ \} = \mathcal{R}_{B_i} m(\beta).$$

Thus the post-block target is the Horvitz-Thompson selected vector, and $\mathcal{R}_{B_i} m(\beta)$ is generally not the full mean field $m(\beta)$. Averaging over the current public block gives

$$\mathbb{E} \{ \tilde{g}_i(\beta) \mid \mathcal{O}_i, \mathcal{H}_{i-1} \} = g_\beta(\mathcal{O}_i), \quad \mathbb{E} \{ \tilde{g}_i(\beta) \mid \mathcal{H}_{i-1} \} = m(\beta). \quad (13)$$

Consequently, for any predictable query point β , $\xi_i(\beta) = \tilde{g}_i(\beta) - m(\beta)$ is a martingale-difference input relative to \mathcal{H}_{i-1} , but not relative to the realized current block. The estimator is (3); public scalar normalizations used in implementations are absorbed into the step-size constant.

The assumptions below separate the standard QR and stochastic-approximation requirements from the finite-channel property proved in Section 2.

Condition 1 (Population QR regularity). *The observations $\mathcal{O}_i = (X_i, Y_i)$ are i.i.d.; $p + 1$ is fixed; $X = (\mathbf{1}, W^\top)^\top$ with $W \in [-1, 1]^p$; and $\mathcal{B} \subset \mathbb{R}^{p+1}$ is compact and convex with β^* in its interior. The risk $M(\beta) = \mathbb{E} \{ \rho_\tau(Y - X^\top \beta) \}$ is finite on \mathcal{B} , and β^* is the unique minimizer. Moreover, for every $\delta > 0$,*

$$\inf_{\beta \in \mathcal{B}: \|\beta - \beta^*\| \geq \delta} (\beta - \beta^*)^\top m(\beta) > 0.$$

In a neighborhood of $X^\top \beta^$, the conditional distribution $Y | X$ has a density $f_{Y|X}(\cdot | X)$ that is uniformly bounded and uniformly locally Lipschitz in its first argument, and the Hessian H in (2) is positive definite.*

Condition 2 (Fixed finite decoded channel). *The LDP channel is a fixed public $\mathbf{CQ}_X(q, s)$ design with $q < \infty$, $1 \leq s \leq p + 1$, and fixed $\varepsilon > 0$. For predictable queries, (13) holds. In addition, the decoded range is uniformly bounded and, under a common coupling of the public channel randomness, there is a constant $C < \infty$ such that, for β, β' in a neighborhood of β^* ,*

$$\mathbb{E} \{ \|\tilde{g}_i(\beta) - \tilde{g}_i(\beta')\|^2 \} \leq C \|\beta - \beta'\|.$$

Condition 3 (ASGD schedule). *The initial value $\beta_0 \in \mathcal{B}$ is public. The step sizes are public and satisfy $\eta_i = \eta_0 i^{-\gamma}$, $\eta_0 > 0$, $\gamma \in (1/2, 1)$.*

Condition 4 (Rank conditions for inference). *Let*

$$\Omega_\varepsilon = \text{Var} \{ \tilde{g}_i(\beta^*) \}, \quad \Sigma_\varepsilon = H^{-1} \Omega_\varepsilon H^{-1}.$$

A scalar contrast $a^\top \beta^$ is reported only when $a^\top \Sigma_\varepsilon a > 0$. A full-vector ellipsoid is reported only when the corresponding limiting covariance or empirical self-normalizer is nonsingular. Group-based Hotelling sets require more group centers than the target dimension and a full-rank empirical group covariance.*

Condition 1 is the usual fixed-dimensional QR regularity framework: bounded covariates, an interior identified target, local smoothness of the conditional density near the target hyperplane, and a nonsingular QR Hessian [Koenker and Bassett, 1978, Koenker, 2005, Angrist et al., 2006, Chernozhukov and Fernández-Val, 2011]. Condition 2 is not an additional modeling assumption: for every fixed finite $\mathbf{CQ}_X(q, s)$ channel, Proposition 1 gives LDP, unbiased decoding, and bounded range, while the displayed local stability follows from the finite decoded range and the QR slab probability bound implied by the density condition. Condition 3 is the standard Polyak-Ruppert averaging schedule [Ruppert, 1988, Polyak and Juditsky,

1992, Kushner and Yin, 2003, Bottou et al., 2018, Gadat and Panloup, 2023]. Condition 4 only excludes degenerate contrasts and singular covariance estimates, as in ordinary studentized and Hotelling inference [Shao, 2010, 2015, Su and Zhu, 2023].

Under Condition 1, the population mean field has the local expansion

$$m(\beta) = H(\beta - \beta^*) + O(\|\beta - \beta^*\|^2), \quad \beta \rightarrow \beta^*.$$

Together with (13), this yields a standard averaged stochastic-approximation problem with bounded martingale noise; the technical verification is deferred to the supplementary proof document. The asymptotic properties are as follows.

Theorem 1 (Consistency). *Suppose Conditions 1-3 hold for a fixed finite $\text{CQ}_X(q, s)$ channel with $q < \infty$, $1 \leq s \leq p + 1$, and $\varepsilon > 0$. Then the recursion (3) satisfies*

$$\beta_i \rightarrow \beta^*, \quad \bar{\beta}_n \rightarrow \beta^*,$$

in probability.

Theorem 2 (Polyak-Ruppert representation and CLT). *Suppose the assumptions of Theorem 1 hold. Define $\xi_i^* = \tilde{g}_i(\beta^*) - m(\beta^*) = \tilde{g}_i(\beta^*)$, $\Omega_\varepsilon = \text{Var}(\xi_i^*)$. Then*

$$\bar{\beta}_n - \beta^* = -H^{-1} \frac{1}{n} \sum_{i=1}^n \xi_i^* + o_p(n^{-1/2}), \quad (14)$$

and hence

$$\sqrt{n}(\bar{\beta}_n - \beta^*) \Rightarrow N(0, H^{-1} \Omega_\varepsilon H^{-1}). \quad (15)$$

The variance Ω_ε is taken over the observation, the public block draw, the stochastic quantization, and the randomized-response step.

The matrix Ω_ε combines ordinary QR estimating-equation variability with the additional variability from local randomization. Thus local privacy changes the estimator covariance, but not the first-order target, because the decoded input is conditionally mean preserving.

3.2 Online Inference Procedures

The CLT in Theorem 2 involves the QR Hessian H . Estimating H under LDP would require additional locally private density or second-order information. We therefore use three Hessian-free procedures that studentize the decoded private trajectory itself: trajectory self-normalization (SN), divide-and-conquer group studentization (DC), and hierarchical group studentization (HiGrad). The inferential target is fixed before data collection: a scalar contrast $a^\top \beta^*$, a coordinate $e_j^\top \beta^*$, a vector contrast $A\beta^*$, or the full coefficient vector β^* .

SN: For $1 \leq \ell \leq n$, write $\bar{\beta}_\ell = \ell^{-1} \sum_{i=1}^\ell \beta_i$. At $t = 0$, define the process below to be zero.

Theorem 3 (Self-normalized inference and functional CLT). *Suppose Conditions 1-4 hold for a fixed finite CQ_X(q, s) channel. Let \mathbb{W}_{p+1} be standard (p + 1)-dimensional Brownian motion. Then, in $D[0, 1]^{p+1}$,*

$$\left\{ \frac{\lfloor nt \rfloor}{\sqrt{n}} (\bar{\beta}_{\lfloor nt \rfloor} - \beta^*) : 0 \leq t \leq 1 \right\} \Rightarrow -H^{-1} \Omega_\varepsilon^{1/2} \mathbb{W}_{p+1}(t).$$

Define the self-normalizer

$$\widehat{V}_n^{\text{SN}} = \frac{1}{n^2} \sum_{\ell=1}^n \ell^2 (\bar{\beta}_\ell - \bar{\beta}_n) (\bar{\beta}_\ell - \bar{\beta}_n)^\top. \quad (16)$$

For any fixed $a \in \mathbb{R}^{p+1}$ with $a^\top \Sigma_\varepsilon a > 0$, let \mathbb{W} be standard one-dimensional Brownian motion and set

$$\mathcal{T}_{\text{SN}} = \frac{\mathbb{W}(1)}{\left[\int_0^1 \{ \mathbb{W}(t) - t\mathbb{W}(1) \}^2 dt \right]^{1/2}}.$$

Then

$$T_n^{\text{SN}}(a) = \frac{\sqrt{n} a^\top (\bar{\beta}_n - \beta^*)}{\left(a^\top \widehat{V}_n^{\text{SN}} a \right)^{1/2}} \Rightarrow \mathcal{T}_{\text{SN}}. \quad (17)$$

If $c_{\text{SN}}(1 - \alpha_{\text{ci}})$ denotes the $(1 - \alpha_{\text{ci}})$ -quantile of $|\mathcal{T}_{\text{SN}}|$, then

$$C_{a, 1-\alpha_{\text{ci}}}^{\text{SN}} = \left[a^\top \bar{\beta}_n \pm c_{\text{SN}}(1 - \alpha_{\text{ci}}) \sqrt{\frac{a^\top \widehat{V}_n^{\text{SN}} a}{n}} \right] \quad (18)$$

has asymptotic coverage $1 - \alpha_{\text{ci}}$ for $a^\top \beta^*$.

For full-vector inference, let $\mathbb{B}_{p+1}(t) = \mathbb{W}_{p+1}(t) - t\mathbb{W}_{p+1}(1)$ be a $(p + 1)$ -dimensional Brownian bridge and define

$$\mathcal{Q}_{\text{SN}, p+1} = \mathbb{W}_{p+1}(1)^\top \left[\int_0^1 \mathbb{B}_{p+1}(t) \mathbb{B}_{p+1}(t)^\top dt \right]^{-1} \mathbb{W}_{p+1}(1).$$

If $\widehat{V}_n^{\text{SN}}$ is nonsingular with probability tending to one, then

$$n (\bar{\beta}_n - \beta^*)^\top \left(\widehat{V}_n^{\text{SN}} \right)^{-1} (\bar{\beta}_n - \beta^*) \Rightarrow \mathcal{Q}_{\text{SN}, p+1}.$$

Thus, with $c_{\text{SN}, p+1}(1 - \alpha_{\text{ci}})$ denoting the corresponding quantile, the ellipsoid

$$C_{1-\alpha_{\text{ci}}}^{\text{SN}} = \left\{ \beta \in \mathbb{R}^{p+1} : n (\bar{\beta}_n - \beta)^\top \left(\widehat{V}_n^{\text{SN}} \right)^{-1} (\bar{\beta}_n - \beta) \leq c_{\text{SN}, p+1}(1 - \alpha_{\text{ci}}) \right\} \quad (19)$$

has asymptotic coverage $1 - \alpha_{\text{ci}}$ when the rank condition holds.

SN uses a single decoded ASGD trajectory and estimates scale from the time variation of its own Polyak averages. The limiting critical values are universal Brownian-bridge functionals and can be simulated once offline; no estimate of H or Ω_ε is required [Shao, 2010, 2015, Fang et al., 2018, Lee et al., 2022].

DC: DC partitions the stream into public disjoint groups before data collection. Each user belongs to exactly one group, so privacy remains the same one-report user-level ε -LDP guarantee. Let the number of groups be R_{DC} , and let the group sizes n_g^{DC} differ by at most one. Run Algorithm 1 independently on each group and let $\widehat{\beta}_1^{\text{DC}}, \dots, \widehat{\beta}_{R_{\text{DC}}}^{\text{DC}}$ be the terminal group Polyak averages. Define

$$\widehat{\beta}^{\text{DC}} = \frac{1}{R_{\text{DC}}} \sum_{g=1}^{R_{\text{DC}}} \widehat{\beta}_g^{\text{DC}}, \quad \widehat{\Sigma}_{\beta}^{\text{DC}} = \frac{1}{R_{\text{DC}} - 1} \sum_{g=1}^{R_{\text{DC}}} \left(\widehat{\beta}_g^{\text{DC}} - \widehat{\beta}^{\text{DC}} \right) \left(\widehat{\beta}_g^{\text{DC}} - \widehat{\beta}^{\text{DC}} \right)^{\top}. \quad (20)$$

For a contrast matrix $A \in \mathbb{R}^{k_A \times (p+1)}$, set $\widehat{\psi}_g^{\text{DC}} = A \widehat{\beta}_g^{\text{DC}}$, $\widehat{\psi}^{\text{DC}} = R_{\text{DC}}^{-1} \sum_{g=1}^{R_{\text{DC}}} \widehat{\psi}_g^{\text{DC}}$, and let $\widehat{\Sigma}_A^{\text{DC}}$ be the empirical covariance matrix of $\widehat{\psi}_1^{\text{DC}}, \dots, \widehat{\psi}_{R_{\text{DC}}}^{\text{DC}}$. When $R_{\text{DC}} > k_A$ and $\widehat{\Sigma}_A^{\text{DC}}$ is full rank, the DC Hotelling set for $\psi = A\beta^*$ is

$$C_{A, 1-\alpha_{\text{ci}}}^{\text{DC}} = \left\{ \psi \in \mathbb{R}^{k_A} : R_{\text{DC}} \left(\widehat{\psi}^{\text{DC}} - \psi \right)^{\top} \left(\widehat{\Sigma}_A^{\text{DC}} \right)^{-1} \left(\widehat{\psi}^{\text{DC}} - \psi \right) \leq c_{k_A, R_{\text{DC}}, \alpha_{\text{ci}}}^{\text{DC}} \right\}, \quad (21)$$

where

$$c_{k_A, R_{\text{DC}}, \alpha_{\text{ci}}}^{\text{DC}} = \frac{k_A (R_{\text{DC}} - 1)}{R_{\text{DC}} - k_A} F_{k_A, R_{\text{DC}} - k_A} (1 - \alpha_{\text{ci}}). \quad (22)$$

Here $F_{\nu_1, \nu_2} (1 - \alpha_{\text{ci}})$ is the $(1 - \alpha_{\text{ci}})$ -quantile of the F distribution with (ν_1, ν_2) degrees of freedom. The coefficient ellipsoid is the special case $A = I_{p+1}$, requiring $R_{\text{DC}} > p + 1$.

For a scalar contrast $a^{\top} \beta^*$,

$$a^{\top} \widehat{\beta}^{\text{DC}} \pm t_{R_{\text{DC}}-1} (1 - \alpha_{\text{ci}}/2) \sqrt{\frac{\widehat{\sigma}_{a, \text{DC}}^2}{R_{\text{DC}}}}, \quad \widehat{\sigma}_{a, \text{DC}}^2 = a^{\top} \widehat{\Sigma}_{\beta}^{\text{DC}} a, \quad (23)$$

is reported when $\widehat{\sigma}_{a, \text{DC}}^2 > 0$, where $t_{\nu} (1 - \alpha_{\text{ci}}/2)$ denotes the corresponding Student- t quantile.

HiGrad: HiGrad uses a public tree to produce multiple correlated group centers whose correlation pattern is known from the tree. Let the branching vector be $\mathbf{b}_{\text{HG}} = (b_1, \dots, b_{L_{\text{HG}}})$, $R_{\text{HG}} = \prod_{\ell=1}^{L_{\text{HG}}} b_{\ell}$, where R_{HG} is the number of leaves. The tree and all segment allocations are fixed before data collection. Let $\nu_{\ell}^{\text{HG}}(r)$ be the ancestor of leaf r at level ℓ . Each tree segment (ℓ, ν) receives a public disjoint subset of users and produces a decoded ASGD segment estimate $\widehat{\beta}_{\ell, \nu}^{\text{seg}}$. With public weights w_{ℓ}^{HG} satisfying $\sum_{\ell=1}^{L_{\text{HG}}} w_{\ell}^{\text{HG}} = 1$, define the leaf estimates

$$\widehat{\beta}_r^{\text{HG}} = \sum_{\ell=1}^{L_{\text{HG}}} w_{\ell}^{\text{HG}} \widehat{\beta}_{\ell, \nu_{\ell}^{\text{HG}}(r)}^{\text{seg}}, \quad r = 1, \dots, R_{\text{HG}}. \quad (24)$$

Let

$$\widehat{\beta}^{\text{HG}} = \frac{1}{R_{\text{HG}}} \sum_{r=1}^{R_{\text{HG}}} \widehat{\beta}_r^{\text{HG}}, \quad L_{\beta}^{\text{HG}} = \begin{pmatrix} \left(\widehat{\beta}_1^{\text{HG}} \right)^{\top} \\ \vdots \\ \left(\widehat{\beta}_{R_{\text{HG}}}^{\text{HG}} \right)^{\top} \end{pmatrix}.$$

Let $\mathbf{1}_{R_{\text{HG}}}$ be the R_{HG} -vector of ones. The shared prefixes induce a public covariance template Σ_{tree} . In the balanced implementation, one concrete template is

$$(\Sigma_{\text{tree}})_{rr'} = \sum_{\ell=1}^{L_{\text{HG}}} \frac{(w_{\ell}^{\text{HG}})^2}{n_{\ell, \nu_{\ell}^{\text{HG}}(r)}} \mathbf{1} \{ \nu_{\ell}^{\text{HG}}(r) = \nu_{\ell}^{\text{HG}}(r') \}, \quad (25)$$

where $n_{\ell, \nu}$ is the size of segment (ℓ, ν) . Let Σ_{tree}^+ be the Moore-Penrose inverse on the centered leaf subspace, and define

$$\sigma_{\text{HG}}^2 = R_{\text{HG}}^{-2} \mathbf{1}_{R_{\text{HG}}}^{\top} \Sigma_{\text{tree}} \mathbf{1}_{R_{\text{HG}}}. \quad (26)$$

Here σ_{HG}^2 is a public tree-design multiplier, distinct from the data-estimated contrast variance $\hat{\sigma}_{a, \text{HG}}^2$ below.

For a scalar contrast a , define $\chi_r(a) = a^{\top} \hat{\beta}_r^{\text{HG}}$, $\bar{\chi}(a) = R_{\text{HG}}^{-1} \sum_{r=1}^{R_{\text{HG}}} \chi_r(a)$, and

$$\hat{\sigma}_{a, \text{HG}}^2 = \frac{1}{R_{\text{HG}} - 1} \{ \chi(a) - \bar{\chi}(a) \mathbf{1}_{R_{\text{HG}}} \}^{\top} \Sigma_{\text{tree}}^+ \{ \chi(a) - \bar{\chi}(a) \mathbf{1}_{R_{\text{HG}}} \}. \quad (27)$$

Provided $\hat{\sigma}_{a, \text{HG}}^2 > 0$, the HiGrad scalar interval is

$$a^{\top} \hat{\beta}^{\text{HG}} \pm t_{R_{\text{HG}}-1} (1 - \alpha_{\text{ci}}/2) \sqrt{\hat{\sigma}_{a, \text{HG}}^2 \sigma_{\text{HG}}^2}. \quad (28)$$

For vector inference, define the centered leaf residual matrix $\tilde{L}_{\beta}^{\text{HG}} = L_{\beta}^{\text{HG}} - \mathbf{1}_{R_{\text{HG}}} \left(\hat{\beta}^{\text{HG}} \right)^{\top}$ and the whitened covariance estimator

$$\hat{\Gamma}_{\beta}^{\text{HG}} = \frac{1}{R_{\text{HG}} - 1} \left(\tilde{L}_{\beta}^{\text{HG}} \right)^{\top} \Sigma_{\text{tree}}^+ \tilde{L}_{\beta}^{\text{HG}}. \quad (29)$$

When $R_{\text{HG}} > p + 1$ and $\hat{\Gamma}_{\beta}^{\text{HG}}$ is full rank, the HiGrad coefficient ellipsoid is

$$C_{1-\alpha_{\text{ci}}}^{\text{HG}} = \left\{ \beta \in \mathbb{R}^{p+1} : (\sigma_{\text{HG}}^2)^{-1} \left(\hat{\beta}^{\text{HG}} - \beta \right)^{\top} \left(\hat{\Gamma}_{\beta}^{\text{HG}} \right)^{-1} \left(\hat{\beta}^{\text{HG}} - \beta \right) \leq c_{p+1, R_{\text{HG}}, \alpha_{\text{ci}}}^{\text{HG}} \right\}, \quad (30)$$

where

$$c_{p+1, R_{\text{HG}}, \alpha_{\text{ci}}}^{\text{HG}} = \frac{(p+1)(R_{\text{HG}}-1)}{R_{\text{HG}}-(p+1)} F_{p+1, R_{\text{HG}}-(p+1)}(1-\alpha_{\text{ci}}). \quad (31)$$

The following corollary records the asymptotic calibration used by the DC and HiGrad procedures. The segment-wise ASGD representations are consequences of Theorem 2 applied to public substreams; they are not additional high-level assumptions. The remaining assumptions are design-balance and rank conditions needed by the Student and Hotelling critical values.

Corollary 1. *Suppose Conditions 1–4 hold for a fixed finite $\text{CQ}_X(q, s)$ channel. All public group and segment recursions below are initialized at public points in \mathcal{B} and use the ASGD schedule $\eta_t = \eta_0 t^{-\gamma}$ in their own local time $t = 1, 2, \dots$*

For DC, let R_{DC} be fixed, let $\mathcal{I}_g^{\text{DC}}$ be public disjoint groups independent of the records, and put $m_n^{\text{DC}} = n/R_{\text{DC}}$. Assume $\min_g n_g^{\text{DC}} \rightarrow \infty$, $\max_{1 \leq g \leq R_{\text{DC}}} |n_g^{\text{DC}}/m_n^{\text{DC}} - 1| \rightarrow 0$. Then there exist remainders $r_{g,n}^{\text{DC}}$ such that, uniformly over the fixed set of groups,

$$\widehat{\beta}_g^{\text{DC}} - \beta^* = -H^{-1} \frac{1}{n_g^{\text{DC}}} \sum_{i \in \mathcal{I}_g^{\text{DC}}} \xi_i^* + r_{g,n}^{\text{DC}}, \quad \max_g \sqrt{n_g^{\text{DC}}} \|r_{g,n}^{\text{DC}}\| \xrightarrow{p} 0.$$

In particular, for any fixed contrast matrix A , $\max_g \sqrt{m_n^{\text{DC}}} \|Ar_{g,n}^{\text{DC}}\| \xrightarrow{p} 0$. If $\Sigma_A = A\Sigma_\varepsilon A^\top$ is positive definite and $R_{\text{DC}} > k_A$, the statistic in (21) converges to the Hotelling law used in (22), and $\Pr\{A\beta^* \in C_{A,1-\alpha_{\text{ci}}}^{\text{DC}}\} \rightarrow 1 - \alpha_{\text{ci}}$. For any scalar contrast a with $a^\top \Sigma_\varepsilon a > 0$, the DC pivot in (23) converges to $t_{R_{\text{DC}}-1}$, so the scalar interval has asymptotic coverage $1 - \alpha_{\text{ci}}$.

For HiGrad, let the branching vector and weights be fixed, let $\mathcal{I}_{\ell,\nu}^{\text{HG}}$ be public disjoint segment sets independent of the records, and assume $\min_{\ell,\nu} n_{\ell,\nu} \rightarrow \infty$. Then there exist remainders $r_{\ell,\nu,n}^{\text{HG}}$ such that, uniformly over the fixed set of tree segments,

$$\widehat{\beta}_{\ell,\nu}^{\text{seg}} - \beta^* = -H^{-1} \frac{1}{n_{\ell,\nu}} \sum_{i \in \mathcal{I}_{\ell,\nu}^{\text{HG}}} \xi_i^* + r_{\ell,\nu,n}^{\text{HG}}, \quad \max_{\ell,\nu} \sqrt{n_{\ell,\nu}} \|r_{\ell,\nu,n}^{\text{HG}}\| \xrightarrow{p} 0.$$

Assume $\sigma_{\text{HG},n}^2 > 0$ eventually and $M_n = \Sigma_{\text{tree},n}/\sigma_{\text{HG},n}^2 \rightarrow M$, where M has constant row sums and is positive definite on the centered leaf subspace. Then the weighted leaf-scale segment remainders are automatically negligible:

$$\max_{1 \leq r \leq R_{\text{HG}}} \frac{1}{\sigma_{\text{HG},n}} \left\| \sum_{\ell=1}^{L_{\text{HG}}} w_\ell^{\text{HG}} r_{\ell,\nu_\ell^{\text{HG}}(r),n}^{\text{HG}} \right\| \xrightarrow{p} 0.$$

Consequently, for any scalar contrast a with $a^\top \Sigma_\varepsilon a > 0$, the HiGrad pivot underlying (28) converges to $t_{R_{\text{HG}}-1}$, and the scalar interval has asymptotic coverage $1 - \alpha_{\text{ci}}$. If Σ_ε is positive definite and $R_{\text{HG}} > p + 1$, the quadratic form in (30) converges to the Hotelling law used in (31), and

$$\Pr\{\beta^* \in C_{1-\alpha_{\text{ci}}}^{\text{HG}}\} \rightarrow 1 - \alpha_{\text{ci}}.$$

SN, DC, and HiGrad estimate scale from decoded private outputs in different ways: SN uses temporal variation in one trajectory and is calibrated by Theorem 3; DC uses independent public groups under the balanced-group condition in Corollary 1; and HiGrad uses a public tree with a known shared-prefix covariance template under the stated convergence, constant-row-sum, and centered-rank conditions. All three are post-processing procedures requiring no additional raw-data access or LDP reports, and Algorithms 2–4 summarize their implementations.

Algorithm 2 Online LDP QR inference via SN

1. **Input.** Stored decoded ASGD averages $\{\bar{\beta}_\ell : 1 \leq \ell \leq n\}$, target contrast a or vector target, and nominal level $1 - \alpha_{\text{ci}}$.
 2. Compute $\widehat{V}_n^{\text{SN}}$ from (16).
 3. For a scalar contrast $a^\top \beta^*$, compute $a^\top \widehat{V}_n^{\text{SN}} a$. If it is positive, report the interval (18).
 4. For a coefficient ellipsoid, check whether $\widehat{V}_n^{\text{SN}}$ is full rank. If so, report (19).
 5. **Output.** SN intervals or ellipsoids.
-

Algorithm 3 Online LDP QR inference via DC

1. **Input.** Public number of groups R_{DC} , channel design (q, s, ε) , ASGD settings, target a or A , and nominal level $1 - \alpha_{\text{ci}}$.
 2. Partition users into R_{DC} disjoint public groups with nearly equal sizes.
 3. Run the decoded ASGD recursion separately on each group and compute terminal group averages $\widehat{\beta}_g^{\text{DC}}$.
 4. Compute $\widehat{\beta}^{\text{DC}}$ and $\widehat{\Sigma}_\beta^{\text{DC}}$ from (20).
 5. For scalar targets, report (23) when the scalar variance is positive.
 6. For vector targets, report (21) when $R_{\text{DC}} > k_A$ and $\widehat{\Sigma}_A^{\text{DC}}$ is full rank.
 7. **Output.** DC intervals or Hotelling sets.
-

3.3 Effective Information and High-Privacy-Budget Recovery

The preceding results are fixed- ε , fixed-finite-channel statements. For interpreting finite-sample behavior, it is useful to make the randomized-response attenuation explicit. For binary randomized response, define $\kappa_{\text{bin}}(\varepsilon) = \tanh(\varepsilon/2)$. A one-coordinate binary decoded input has variance inflation of order $\kappa_{\text{bin}}(\varepsilon)^{-2}$, with $\kappa_{\text{bin}}(\varepsilon)^2 \sim \varepsilon^2/4$ as $\varepsilon \downarrow 0$. If coordinate j is selected with public probability π_j , a first-order coordinate information index is

$$n_{\text{eff},j} = n\pi_j\kappa_{\text{bin}}(\varepsilon)^2, \quad n_{\text{eff}}^{\min} = \min_{0 \leq j \leq p} n_{\text{eff},j}. \quad (32)$$

Algorithm 4 Online LDP QR inference via HiGrad

1. **Input.** Public branching vector \mathbf{b}_{HG} , public segment allocations, public weights w_ℓ^{HG} , channel design (q, s, ε) , ASGD settings, target a or full vector, and nominal level $1 - \alpha_{\text{ci}}$.
2. For each tree segment (ℓ, ν) , run decoded ASGD on the users assigned to that segment and compute $\widehat{\beta}_{\ell, \nu}^{\text{seg}}$.
3. For each leaf r , form $\widehat{\beta}_r^{\text{HG}}$ using (24).
4. Compute $\widehat{\beta}^{\text{HG}}$, the tree template Σ_{tree} , and σ_{HG}^2 .
5. For scalar targets, compute $\widehat{\sigma}_{a, \text{HG}}^2$ and report (28) when it is positive.
6. For coefficient ellipsoids, compute $\widehat{\Gamma}_\beta^{\text{HG}}$ and report (30) when $R_{\text{HG}} > p + 1$ and $\widehat{\Gamma}_\beta^{\text{HG}}$ is full rank.
7. **Output.** HiGrad intervals or ellipsoids.

For a joint block with alphabet size K_B , using the attenuation factor $\kappa_{\text{tr}}(K_B, \varepsilon)$ defined in (9), the analogous coordinate-level index is

$$n_{\text{eff}, j}^{\text{blk}} = n \mathbb{E}_B \{ \mathbf{1}(j \in B) \kappa_{\text{tr}}(K_B, \varepsilon)^2 \}, \quad n_{\text{eff}}^{\text{blk}, \min} = \min_{0 \leq j \leq p} n_{\text{eff}, j}^{\text{blk}}.$$

These indices do not replace the covariance Ω_ε , but they help diagnose slow convergence when ε is small, the selected block is sparse, or the randomized-response alphabet is large.

Finally, the nonprivate online QR recursion is recovered along high-privacy-budget and high-resolution design paths.

Corollary 2 (High- ε recovery). *Consider a public design path $\text{CQ}_X(q_\varepsilon, s_\varepsilon)$ such that $s_\varepsilon = p + 1$ eventually, $q_\varepsilon \rightarrow \infty$, and $\kappa_{\text{tr}}(K_\varepsilon, \varepsilon) \rightarrow 1, K_\varepsilon = 2q_\varepsilon^p$ once $s_\varepsilon = p + 1$. Then, for each fixed β in a neighborhood of β^* , $\widetilde{g}_{\theta_\varepsilon}(\beta) \rightarrow g_\beta(\mathcal{O})$ in L^2 .*

Under Condition 1, the convergence is locally uniform over fixed compact neighborhoods of β^ . Moreover, $\Omega_\varepsilon \rightarrow \Omega_0 = \text{Var}\{g_{\beta^*}(\mathcal{O})\}$.*

If the linear conditional quantile model is correctly specified, so that $\Pr(Y \leq X^\top \beta^ | X) = \tau$ almost surely, then $\Omega_0 = \tau(1 - \tau) \mathbb{E}(XX^\top)$. Consequently, the limiting covariance in Theorem 2 approaches the nonprivate ASGD covariance along this path.*

Thus the fixed finite-channel theory describes the private regime, while the corollary clarifies the connection to ordinary nonprivate online QR. At small ε , randomized-response inversion inflates Ω_ε ; at large ε , with sufficiently refined all-coordinate quantization, the decoded input approaches the exact QR estimating-equation contribution.

4 Numerical Experiments

This section evaluates the finite-sample accuracy and inference behavior of the locally private online estimator in controlled simulations. The comparisons focus on the privacy path toward the nonprivate ASGD oracle, the gain from the support-aware mean-preserving channel $\text{CQ}_X(q, s)$, and the calibration of trajectory-based confidence summaries.

All methods use the same streaming data-generating model and projected Polyak-Ruppert recursion. The nonprivate ASGD estimator serves only as an oracle reference, using unperturbed estimating-equation inputs with no local quantization, coordinate selection, or randomized response; finite privacy budgets use $\text{CQ}_X(q, s)$.

4.1 Simulation Setup

For p non-intercept covariates, generate $X_i = (1, W_i^\top)^\top$, $W_{ij} \stackrel{\text{ind}}{\sim} \text{Unif}[-1, 1]$, $j = 1, \dots, p$. The target coefficient is

$$\beta^* = \frac{(1, -2, 3, -4, \dots, (-1)^p (p+1))^\top}{\|(1, -2, 3, -4, \dots, (-1)^p (p+1))^\top\|_2}.$$

The alternating signs and increasing magnitudes make the slope effects heterogeneous across coordinates, while the normalization keeps the signal scale fixed across p . Conditional on X_i , responses are generated by

$$Y_i = X_i^\top \beta^* + 0.5 \{\zeta_i - \log(\tau/(1-\tau))\}, \quad \zeta_i \sim \text{Logistic}(0, 1).$$

Because the τ -quantile of ζ_i is $\log(\tau/(1-\tau))$, the conditional τ -quantile of Y_i given X_i is $X_i^\top \beta^*$. The scale 0.5 fixes the noise level and is held constant across all simulation cells.

The public simulation grid is $\tau \in \{0.5, 0.75\}$, $p \in \{1, 2, 5, 8\}$, $\varepsilon \in \{0.5, 1, 2, 4, 8, 16, \infty\}$. We use value $\varepsilon = \infty$ to denote the separate nonprivate ASGD oracle.

For each finite- ε cell, the local channel is $\text{CQ}_X(q, s)$, with (q, s) selected before final evaluation from a prespecified coordinate-quantized candidate family using independent screening runs with the same synthetic model and step-size template. The selected choices are fixed for final evaluation and reported in Table 2; they are sparse at stringent privacy budgets and become richer through more selected coordinates or finer quantization as ε increases.

4.2 Online Recursion and Reported Summaries

The numerical implementation follows Algorithm 1. For private finite- ε cells, $\tilde{g}_i(\beta_{i-1})$ is the decoded private estimating-equation input produced by the coordinate-quantized channel. For the nonprivate oracle cells, the reference implementation replaces this input by the unperturbed estimating-equation contribution $g_{\beta_{i-1}}(\mathcal{O}_i)$, with no local quantization, coordinate selection, or randomized response. All synthetic runs

τ	p	$\varepsilon = 0.5$	$\varepsilon = 1$	$\varepsilon = 2$	$\varepsilon = 4$	$\varepsilon = 8$	$\varepsilon = 16$
0.50	1	(4,1)	(2,1)	(4,1)	(4,2)	(16,2)	(8,2)
0.50	2	(2,1)	(2,1)	(2,1)	(4,3)	(8,3)	(8,3)
0.50	5	(2,1)	(2,1)	(4,1)	(8,1)	(3,5)	(4,6)
0.50	8	(2,1)	(2,1)	(4,1)	(3,2)	(3,5)	(4,9)
0.75	1	(4,1)	(2,2)	(2,2)	(4,2)	(8,2)	(16,2)
0.75	2	(2,1)	(2,2)	(4,1)	(3,3)	(8,3)	(16,3)
0.75	5	(2,1)	(4,1)	(4,1)	(3,2)	(3,6)	(8,6)
0.75	8	(2,1)	(2,1)	(3,1)	(8,1)	(3,5)	(4,9)

Table 2: Private finite- ε local-channel choices for the $\text{CQ}_X(q, s)$ simulations. Each entry reports (q, s) , where q is the slope-grid size and s is the selected estimating-equation coordinate-block size.

initialize at $\beta_0 = 0$ and use the same coordinate-wise projection set $[-10, 10]^{p+1}$, including the geometric baseline runs.

The simulations use the public stabilized power schedule $\eta_i = r_{\mathcal{M}}/(i^{0.65} + 300)$, with method-specific positive scale $r_{\mathcal{M}}$ fixed before the stream begins. This finite-sample version of the Polyak-Ruppert schedule in Condition 3 uses public scales recorded in Appendix A for replication.

Point-estimation summaries are recorded at the reporting set

$$\mathcal{T} = \{10^3, 3 \times 10^3, 10^4, 3 \times 10^4, 10^5, 3 \times 10^5, 10^6, 3 \times 10^6, 10^7, 3 \times 10^7, 10^8, 3 \times 10^8\}.$$

A simulation cell fixes (τ, p, ε) and, for $\varepsilon < \infty$, the public channel choice (q, s) . The 48 private finite- ε $\text{CQ}_X(q, s)$ cells and 8 nonprivate oracle cells use 500 independent Monte Carlo replications per cell, while the two geometric baselines use 200 replications over the same 48 private cells. Estimation performance is measured by $\|\bar{\beta}_n - \beta^*\|_2$, and uncertainty quantification by empirical coverage of nominal 95% coordinate intervals, dense-contrast intervals for $a_{\text{den}}^\top \beta^*$ with $a_{\text{den}} = (p+1)^{-1/2} \mathbf{1}_{p+1}$, and coefficient ellipsoids. We reserve τ for the quantile level and use α_{ci} for inferential miscoverage, so all intervals and ellipsoids have nominal level $1 - \alpha_{\text{ci}} = 0.95$.

Because each user contributes only one privatized category, nominal stream length differs from usable information: coordinate selection lowers observation frequency for each block, and randomized-response inversion amplifies variation when ε is small. Table 3 therefore reports representative block-level effective-information values and the observed large- n error decay of the averaged recursion, estimated by fitting $\log\{\text{mean } \ell_2 \text{ error}\} = a + b \log n$ over $n \geq 10^6$. Across all 48 finite- ε $\text{CQ}_X(q, s)$ cells, the fitted slopes have median -0.503 , IQR -0.509 to -0.500 , and range -0.531 to -0.491 , so stringent privacy mainly changes the effective-information constant while fixed-channel averaged trajectories retain root- n -type decay.

(τ, p, ε)	(q, s)	$n_{\text{eff}}^{\text{blk}, \text{min}}$	10^6	10^7	10^8	3×10^8	slope b
(0.50, 2, 2)	(2, 1)	5.80×10^7	9.26×10^{-3}	2.81×10^{-3}	8.98×10^{-4}	5.25×10^{-4}	-0.503
(0.75, 8, 0.5)	(2, 1)	2.00×10^6	2.46×10^{-1}	6.70×10^{-2}	2.07×10^{-2}	1.17×10^{-2}	-0.531
(0.50, 8, 16)	(4, 9)	2.91×10^8	5.55×10^{-3}	1.71×10^{-3}	5.47×10^{-4}	3.15×10^{-4}	-0.502
(0.75, 8, 16)	(4, 9)	2.91×10^8	6.67×10^{-3}	2.01×10^{-3}	6.31×10^{-4}	3.69×10^{-4}	-0.505

Table 3: Effective-information and large- n trajectory diagnostic. The $n_{\text{eff}}^{\text{blk}, \text{min}}$ column is computed at $n = 3 \times 10^8$ using the reference contraction in the public step-size rule. The four middle columns report mean Euclidean estimation error at the displayed stream lengths, and b is the fitted log-log slope over $n \geq 10^6$.

4.3 Estimation Accuracy

The estimation summaries move from the privacy-accuracy path to mechanism comparisons. We first vary ε at fixed dimension, then check whether the large- ε behavior remains close to the nonprivate reference as dimension grows, and finally compare against geometric baselines at the final horizon.

At $p = 2$, the privacy path separates the proposed channel from both geometric releases. Direct Laplace is the closest baseline at large ε but remains above the matched $\text{CQ}_X(q, s)$ errors. For $\tau = 0.75$, face-exponential release often drives small- ε paths to the projection boundary because it preserves support without preserving the mean; the errors near 9.8 are therefore boundary-saturation failures rather than ordinary privacy-noise plateaus.

ε	$\text{CQ}_X(q, s)$		Direct Laplace		Face-exponential	
	$\tau = 0.50$	$\tau = 0.75$	$\tau = 0.50$	$\tau = 0.75$	$\tau = 0.50$	$\tau = 0.75$
0.5	1.63×10^{-3}	3.08×10^{-3}	3.57×10^{-3}	5.35×10^{-3}	7.72×10^{-3}	9.85^\times
1	8.30×10^{-4}	1.59×10^{-3}	1.99×10^{-3}	2.63×10^{-3}	3.61×10^{-3}	9.85^\times
2	5.25×10^{-4}	7.26×10^{-4}	9.50×10^{-4}	1.22×10^{-3}	1.99×10^{-3}	9.84^\times
4	2.57×10^{-4}	2.83×10^{-4}	4.84×10^{-4}	6.32×10^{-4}	9.37×10^{-4}	9.81^\times
8	1.50×10^{-4}	1.82×10^{-4}	2.88×10^{-4}	3.41×10^{-4}	4.91×10^{-4}	2.05×10^{-1}
16	1.41×10^{-4}	1.67×10^{-4}	1.87×10^{-4}	2.29×10^{-4}	2.70×10^{-4}	6.74×10^{-3}
∞	1.39×10^{-4}	1.67×10^{-4}	–	–	–	–

Table 4: Mean Euclidean estimation error at $n = 3 \times 10^8$ with $p = 2$, varying the privacy budget and release mechanism. The $\text{CQ}_X(q, s)$ finite- ε rows use the local-channel choices in Table 2. The $\varepsilon = \infty$ row is the common nonprivate ASGD oracle and is not a Laplace or face-exponential release. The $\text{CQ}_X(q, s)$ means use 500 replications per cell, while the two geometric baselines use 200 replications per cell. A superscript \times marks a face-exponential value whose magnitude is dominated by saturation at the projection boundary, rather than by an ordinary privacy-noise plateau.

τ	p	$\text{CQ}_X(q, s), \varepsilon = 16$	nonprivate ASGD	CQ/ASGD
0.50	1	1.03×10^{-4}	1.01×10^{-4}	1.03
0.50	2	1.41×10^{-4}	1.39×10^{-4}	1.02
0.50	5	2.45×10^{-4}	2.25×10^{-4}	1.09
0.50	8	3.15×10^{-4}	2.82×10^{-4}	1.12
0.75	1	1.16×10^{-4}	1.16×10^{-4}	1.00
0.75	2	1.67×10^{-4}	1.67×10^{-4}	1.00
0.75	5	2.60×10^{-4}	2.53×10^{-4}	1.03
0.75	8	3.69×10^{-4}	3.29×10^{-4}	1.12

Table 5: High-budget recovery check at $n = 3 \times 10^8$ with $\varepsilon = 16$, varying p . Rows cover $\tau \in \{0.50, 0.75\}$ and $p \in \{1, 2, 5, 8\}$. The $\text{CQ}_X(q, s)$ rows use the local-channel choices in Table 2. Ratios compare the private finite- ε estimator with the nonprivate ASGD oracle. Each mean is computed over 500 independent Monte Carlo replications.

Table 5 fixes $\varepsilon = 16$ and asks whether the high-budget private channel is already close to the nonprivate ASGD reference as p varies. In these displayed fixed-dimensional cells, the ratios are near one for $p \leq 5$ and about 1.12 at $p = 8$. Thus the later baseline gaps should not be read as a weak proposed reference: at this large budget, $\text{CQ}_X(q, s)$ is already tracking the ASGD oracle closely.

Across the 56 final-horizon $\text{CQ}_X(q, s)$ and nonprivate configurations, Monte Carlo error is small relative to the reported means: the median Monte Carlo standard error is 7.2×10^{-6} , or 1.7% of the corresponding mean error, and the largest relative value is 3.2%. The intermediate-horizon behavior is summarized by the effective-information/root- n diagnostic in Table 3.

The comparison with geometric baselines should be read at the decoded online-update level, not as a claim that every decoded full vector lies in the original two-face support \mathcal{G}_τ . Conditional on the public block B , $\text{CQ}_X(q, s)$ uses the projected support geometry for selected coordinates and then applies an affine randomized-response inverse; this preserves the selected-block mean, and public block sampling recovers the full estimating-equation mean after Horvitz-Thompson reconstruction. Thus, when $s < p + 1$, the tested advantage is support-aware finite-alphabet privatization with mean-preserving decoding, rather than literal full-dimensional support preservation.

Table 6 keeps the same matched baseline comparison but reports where the ratios arise. For each (τ, p) , the displayed ratio summaries are computed over the six finite privacy budgets at $n = 3 \times 10^8$; each ratio is the baseline mean Euclidean error divided by the matched $\text{CQ}_X(q, s)$ mean Euclidean error. A ratio greater than one favors the coordinate-quantized decoded estimator.

τ	p	Direct Laplace/CQ _X		Face-exponential/CQ _X	
		median	range	median	range
0.50	1	1.65	1.09–1.89	3.07	1.39–3.86
0.50	2	1.90	1.32–2.39	3.71	1.91–4.74
0.50	5	2.86	1.81–3.35	5.50	3.37–6.90
0.50	8	3.67	2.57–4.14	7.45	5.07–8.76
0.75	1	1.52	1.10–2.17	$5.70 \times 10^{3 \times}$	$68.5 - 2.93 \times 10^{4 \times}$
0.75	2	1.71	1.37–2.23	$4.69 \times 10^{3 \times}$	$40.2 - 3.46 \times 10^{4 \times}$
0.75	5	3.04	2.73–3.54	$4.21 \times 10^{3 \times}$	$38.4 - 2.49 \times 10^{4 \times}$
0.75	8	4.01	3.52–4.19	$2.75 \times 10^{3 \times}$	$26.8 - 1.52 \times 10^{4 \times}$

Table 6: Matched estimation-only comparison with geometric baselines at $n = 3 \times 10^8$. The entries are baseline-to-CQ_X(q, s) mean-error ratios, not raw errors: the Direct Laplace columns compare Direct Laplace against CQ_X(q, s), and the Face-exponential columns compare Face-exponential against CQ_X(q, s). For each (τ, p), medians and ranges summarize these ratios over $\varepsilon \in \{0.5, 1, 2, 4, 8, 16\}$. Baseline configurations use 200 independent replications, while the CQ_X(q, s) comparison values use 500 independent replications. A superscript \times marks a face-exponential aggregate dominated by cells whose reported errors are governed by projection-boundary saturation.

Over all 48 matched finite- ε cells, the median ratios are 2.31 for Direct Laplace and 17.8 for Face-exponential, with every ratio above one. Direct Laplace is the more stable comparator but its relative cost increases with dimension, whereas Face-exponential is only moderately worse for $\tau = 0.50$ but orders of magnitude worse for $\tau = 0.75$, consistent with mean-field mismatch rather than ordinary privacy-noise inflation.

4.4 Uncertainty Quantification

The coverage experiments ask whether uncertainty can be estimated from the same locally private online trajectory. The primary procedure is SN, calibrated by Theorem 3; we also report DC and HiGrad, both post-processing procedures based on decoded online estimates that require no additional access to raw data.

The inferential targets are coordinate intervals, the dense contrast $a_{\text{den}}^\top \beta^*$, and coefficient ellipsoids at $n = 3 \times 10^8$. DC uses $R_{\text{DC}} = p + 5$ disjoint groups, with $t_{R_{\text{DC}}-1}$ critical values for scalar intervals and the corresponding Hotelling form for vector ellipsoids when the group covariance is full rank. HiGrad is reported for public branching vectors $\mathbf{b}_{\text{HG}} = [4, 4]$, $[4, 8]$, and $[4, 4, 4]$, with 16, 32, and 64 leaves; because leaf estimates share public prefixes, studentization uses the known leaf-correlation template, and ellipsoid summaries are reported only when the covariance-rank condition holds. For nominal 95% SN scalar

τ	Method	coordinate	dense	ellipsoid
0.50	SN	0.934-0.946	0.940	0.934
0.50	DC	0.948-0.966	0.950	0.954
0.50	HiGrad [4, 4]	0.934-0.950	0.956	0.952
0.50	HiGrad [4, 8]	0.946-0.952	0.954	0.952
0.50	HiGrad [4, 4, 4]	0.932-0.940	0.936	0.934
0.75	SN	0.952-0.960	0.962	0.946
0.75	DC	0.884-0.952	0.948	0.936
0.75	HiGrad [4, 4]	0.932-0.944	0.934	0.920
0.75	HiGrad [4, 8]	0.916-0.922	0.918	0.914
0.75	HiGrad [4, 4, 4]	0.904-0.940	0.926	0.896

Table 7: Final empirical 95% coverage at $p = 2$, $\varepsilon = 2$, and $n = 3 \times 10^8$. SN denotes trajectory self-normalization, DC denotes divide-and-conquer disjoint-group studentization, and HiGrad denotes hierarchical group studentization. Coordinate columns report the min-max over the $p + 1 = 3$ coordinate intervals; dense denotes the $a_{\text{den}} = (p + 1)^{-1/2} \mathbf{1}_{p+1}$ contrast; ellipsoid denotes full-coefficient coverage. For HiGrad, \mathbf{b}_{HG} denotes the public branching vector; $\mathbf{b}_{\text{HG}} = [4, 4]$, $[4, 8]$, and $[4, 4, 4]$, have $R_{\text{HG}} = 16$, 32 , and 64 leaves, respectively. Each displayed coverage estimate is computed from 500 independent Monte Carlo replications, giving Monte Carlo standard error at most 0.023.

procedures, the Brownian-bridge critical value is 6.7134; for SN coefficient ellipsoids with $p + 1 = 2, 3, 6, 9$, the critical values are 103.584, 174.998, 464.956, 864.991, computed as Monte Carlo 0.95 quantiles of the Brownian-bridge quadratic-form limits using 200000 paths, 1000 grid points, and a fixed seed.

Table 7 reports a moderate private configuration, $p = 2$ and $\varepsilon = 2$, at the final horizon. The three HiGrad trees are shown separately because the public tree determines the finite-sample studentization.

For $\tau = 0.50$, all reported methods are close to nominal coverage for coordinate intervals, the dense contrast, and coefficient ellipsoids. For $\tau = 0.75$, SN remains close to nominal, while DC and HiGrad show some undercoverage for particular coordinate and ellipsoid summaries; dense-contrast coverage is more stable than the least favorable coordinate and full-vector summaries. The upper-quantile, higher-dimensional, low-privacy-budget configuration $(\tau, p, \varepsilon) = (0.75, 8, 0.5)$ strengthens the same pattern: scalar dense-contrast coverage remains comparatively stable, whereas coordinate intervals and coefficient ellipsoids are more sensitive to finite effective information and covariance conditioning. The reported ellipsoid rows satisfy the required covariance-rank conditions, so the degradation reflects finite-sample conditioning rather than omitted rank failures.

The main empirical message is simple: once the effective-information index is large enough, the decoded $\text{CQ}_X(q, s)$ recursion tracks the nonprivate ASGD reference and outperforms the geometric baselines. The inference summaries reinforce the contrast-specific stability described above.

5 Real-Data: New York City Taxi Trips

We next evaluate the online recursion on January 2024 New York City yellow-taxi trip records released by the New York City Taxi and Limousine Commission [New York City Taxi and Limousine Commission, 2024]. Each record contains pickup and dropoff timestamps, pickup and dropoff taxi-zone identifiers, trip distance, passenger count, and fare components, making the stream a natural illustration of the one-record, one-report local protocol: a trip record is treated as the sensitive contribution, records are timestamped, and the server processes them in chronological order without repeated interaction with the same record-level contributor. The illustration should not be read as a person-level guarantee for individuals who may appear in multiple trip records.

5.1 Data Construction

The response is

$$Y = \log \{1 + \text{trip duration in minutes}\},$$

where duration is computed from the pickup and dropoff timestamps. The downloaded January file contains 2,964,624 raw trip records. We retain trips with pickup time in January 2024, duration between 1 and 180 minutes, positive trip distance no larger than 100 miles, positive fare amount, passenger count in $\{1, \dots, 6\}$, and nonmissing pickup and dropoff locations. This leaves $n = 2,713,434$ trips. Table 8 summarizes the retained stream.

Quantity	Value
Raw January 2024 yellow-taxi records	2,964,624
Retained records after cleaning	2,713,434
Training / test split sizes	2,062,859 / 650,575
Random split seed	2026061903
Trip duration Q1/median/Q3 (minutes)	7.25 / 11.65 / 18.68
Trip distance Q1/median/Q3 (miles)	1.01 / 1.70 / 3.13
Mean passenger count	1.35
Weekend pickups	25.3%
JFK/LGA pickup / dropoff	8.2% / 1.9%
Manhattan pickups	89.7%

Table 8: Summary of the retained New York City yellow-taxi stream used in the real-data illustration. Q1 and Q3 denote the first and third empirical quartiles.

The covariate vector has $p = 8$ non-intercept coordinates: clipped and rescaled $\log(1 + \text{trip distance})$, sine and cosine transforms of pickup hour, a weekend indicator, passenger count scaled from $1, \dots, 6$ to

$[-1, 1]$, JFK/LGA airport pickup and dropoff indicators, and a Manhattan pickup indicator. The distance feature is clipped at 20 miles before scaling, all non-intercept coordinates lie in $[-1, 1]$, and the resulting target is a descriptive streaming linear QR projection for these clipped and publicly scaled features rather than a causal model for trip duration.

5.2 Holdout Calibration and Stability

Because the real-data population coefficient is unknown, we evaluate holdout calibration rather than coefficient coverage. We sample 650,575 retained trips as a uniform holdout and process the remaining 2,062,859 trips once in pickup-time order. For each $\hat{\beta}_\tau$, we report the hit rate

$$\hat{c}_\tau = n_{\text{test}}^{-1} \sum_{i \in \text{test}} \mathbf{1} \left(Y_i \leq X_i^\top \hat{\beta}_\tau \right),$$

and the test check loss. The nonprivate reference hit rates, 0.445 for $\tau = 0.50$ and 0.672 for $\tau = 0.75$, indicate misspecification of the clipped linear projection and one-pass reference; the real-data question is whether private estimates preserve this reference calibration and loss as ε varies.

We use the same $p = 8$ channel choices from Table 2, initialize at zero, set $\eta_i = 0.08i^{-0.75}$, and project coordinatewise onto $[-8, 8]$. Table 9 reports 20 independent repetitions of public block selection, stochastic quantization, and randomized response for each private cell, giving the holdout hit rate, 10^3 times the excess holdout check loss relative to the nonprivate training-stream reference, and the Euclidean distance between the private Polyak average and that reference. Specifically, if $L_{\text{test},\tau}(\beta) = n_{\text{test}}^{-1} \sum_{i \in \text{test}} \rho_\tau(Y_i - X_i^\top \beta)$, the reported loss contrast is $10^3 \Delta_{\text{loss}}$, where $\Delta_{\text{loss}} = L_{\text{test},\tau}(\hat{\beta}_\tau) - L_{\text{test},\tau}(\hat{\beta}_\tau^{\text{np}})$ and $\hat{\beta}_\tau^{\text{np}}$ is the nonprivate one-pass ASGD estimate trained on the same stream.

The holdout results mirror the simulations without requiring a known coefficient. At $\varepsilon = 2$ and 4, private estimates show larger coefficient and excess-loss variation while keeping average hit rates near the nonprivate reference. At $\varepsilon = 8$, excess test losses are close to zero, and at $\varepsilon = 16$ the higher-resolution all-coordinate channel nearly matches the nonprivate stream reference, with hit rates agreeing to three decimals and mean ℓ_2 distances 0.013 and 0.021 for $\tau = 0.50$ and 0.75. Thus larger ε mainly improves preservation of nonprivate holdout calibration and predictive check loss.

We also ran the two geometric baselines from Section 2 on the same real-data split, using the same training stream, holdout set, step-size rule, projection set, privacy budgets, and 20 repetitions per private cell. Table 10 summarizes these 8 finite- ε cells; the same mean/support tradeoff appears in the holdout diagnostics, with the face-exponential shift especially visible for $\tau = 0.75$.

τ	ε	(q, s)	$n_{\text{eff}}^{\text{blk}, \text{min}}$	test hit rate	$10^3 \Delta_{\text{loss}}$	ℓ_2 distance
0.50	2	(4,1)	8.67×10^4	0.450 (0.008)	7.40 (43.31)	0.553 (0.133)
0.50	4	(3,2)	3.40×10^5	0.448 (0.008)	8.92 (17.32)	0.255 (0.068)
0.50	8	(3,5)	1.01×10^6	0.446 (0.002)	-1.18 (8.07)	0.123 (0.042)
0.50	16	(4,9)	2.00×10^6	0.445 (0.000)	0.04 (0.92)	0.013 (0.007)
0.50	∞	–	2.06×10^6	0.445	0.00	0.000
0.75	2	(3,1)	1.06×10^5	0.675 (0.014)	23.23 (47.24)	0.609 (0.253)
0.75	4	(8,1)	1.74×10^5	0.674 (0.012)	12.65 (48.34)	0.475 (0.165)
0.75	8	(3,5)	1.01×10^6	0.673 (0.004)	3.30 (11.07)	0.149 (0.034)
0.75	16	(4,9)	2.00×10^6	0.672 (0.001)	-0.42 (1.21)	0.021 (0.012)
0.75	∞	–	2.06×10^6	0.672	0.00	0.000

Table 9: Holdout calibration and stability for New York City yellow-taxi trips. The test set is a uniform random holdout of 650,575 retained trips, drawn without replacement using public seed 2026061903; the remaining 2,062,859 trips form the training stream. Finite- ε entries are means with Monte Carlo standard deviations in parentheses over 20 repetitions of the local-channel randomness. The $\varepsilon = \infty$ rows are the nonprivate one-pass ASGD references trained on the same training stream.

Method	med. $ \Delta_{\text{hit}} $	med. $10^3 \Delta_{\text{loss}}$	med. ℓ_2	max ℓ_2
$\text{CQ}_X(q, s)$	0.002	5.35	0.202	0.61
Direct Laplace	0.003	20.09	0.654	2.61
Face-exponential	0.328	753.56	3.683	5.93

Table 10: Real-data comparison with geometric baselines over the 8 finite- ε cells. Each entry is a median of cell means, where each private cell mean uses 20 repetitions of the corresponding local randomization. Here Δ_{hit} is the test hit rate minus the nonprivate holdout hit rate at the same τ ; Δ_{loss} is the excess holdout check loss defined above; and the ℓ_2 distance is relative to the nonprivate training-stream reference.

Using the displayed $\text{CQ}_X(q, s)$ row as the calibration scale, the Direct Laplace medians are about 1.8, 3.8, 3.2, and 4.3 times as large for hit-rate deviation, test loss, median ℓ_2 distance, and maximum ℓ_2 distance. The corresponding Face-exponential multipliers are about 208, 141, 18.2, and 9.7.

6 Concluding Remarks

This paper develops a one-report local-privacy framework for online quantile regression. The key step is to view the usual QR update as an unobserved estimating-equation contribution and to replace it by a decoded LDP input with the same conditional mean. The $\text{CQ}_X(q, s)$ channel combines the two-face QR support,

stochastic quantization, randomized response, affine decoding, and Horvitz-Thompson reconstruction. For fixed finite designs, this yields consistent projected Polyak-Ruppert estimation, a central limit theorem, and Hessian-free scalar inference. The simulations and taxi-data illustration show the corresponding privacy-accuracy tradeoff and the benefits of preserving both support structure and mean unbiasedness.

The theory is deliberately fixed-dimensional, with bounded covariates, nonsingular local QR Hessian, public finite-channel choices, and one LDP report per participant. These assumptions yield exact ε -LDP for each participant’s one-record contribution and a clean stochastic-approximation limit, while requiring public scaling or clipping and predictable adaptive choices. Scalar and prespecified low-dimensional inference is the most stable; full ellipsoids are more sensitive to conditioning, rank, and finite effective information.

Extensions such as high-dimensional QR, adaptive channel design, and locally private Hessian or density estimation require new mechanisms, additional reports, stronger modeling assumptions, or new one-report constructions. The main conclusion is that one-report local privacy is compatible with online QR when the report and decoder preserve the estimating-equation mean, at the cost of variance inflation under tighter privacy, larger alphabets, sparse coordinate selection, or higher dimension.

7 Acknowledgments

The authors acknowledge computational resources provided by the Digital Research Alliance of Canada. The authors report no additional funding for this work and no competing interests relevant to this submission.

A Additional Numerical-Experiment Details

This appendix records implementation details for the simulation study in Section 4. The main text reports the primary privacy path, high-budget recovery check, geometry-baseline comparison, and a representative coverage table. The table below gives the public run configuration used for the additional numerical summaries in Appendix B.

A.1 Public Design and Implementation

The public simulation grid is

$$\tau \in \{0.5, 0.75\}, \quad p \in \{1, 2, 5, 8\}, \quad \varepsilon \in \{0.5, 1, 2, 4, 8, 16, \infty\}.$$

The finite- ε $\text{CQ}_X(q, s)$ cells use the public channel choices reported in Table 2 of the main text. These choices were selected before final evaluation from an independent 10^7 -user screening profile over the same synthetic

model and step-size template. The nonprivate $\varepsilon = \infty$ rows use unperturbed QR estimating-equation inputs, all coordinates, no local randomization, and no finite (q, s) channel.

All synthetic streams are generated online. The final $\text{CQ}_X(q, s)$ summaries cover 48 finite- ε private cells plus 8 nonprivate reference cells and use 500 independent Monte Carlo replications per cell. The estimation-only direct Laplace and face-exponential baseline summaries use 200 replications for each of the 96 baseline cells formed by the 48 private finite- ε cells and the two baseline mechanisms. No raw synthetic records are stored as part of the reported summary tables.

The point-estimation summaries report sample sizes

$$\mathcal{T} = \{10^3, 3 \times 10^3, 10^4, 3 \times 10^4, 10^5, 3 \times 10^5, 10^6, 3 \times 10^6, 10^7, 3 \times 10^7, 10^8, 3 \times 10^8\}.$$

For private finite-channel cells, the ASGD recursion uses the public stabilized power schedule

$$\eta_i = \frac{10 \kappa_{\text{ref}}(\varepsilon) \sqrt{s/d}}{i^{0.65} + 300}, \quad d = p + 1,$$

where $s = |B|$, $K_{\text{ref}} = \max_{B:|B|=s} K_B$, and $\kappa_{\text{ref}}(\varepsilon) = \kappa_{\text{rr}}(K_{\text{ref}}, \varepsilon)$. The nonprivate reference uses the same template with all coordinates and $\kappa_{\text{ref}}(\infty) = 1$. All runs initialize at zero and project coordinatewise onto $[-10, 10]^d$.

The inference summaries use trajectory self-normalization (SN), divide-and-conquer studentization (DC), and hierarchical group studentization (HiGrad). DC uses $R_{\text{DC}} = p + 5$ disjoint groups. HiGrad uses the three public branching vectors in Table 11. For the nominal 95% SN procedures, the scalar Brownian-bridge critical value is 6.7134, and the coefficient-ellipsoid SN critical values for $d = 2, 3, 6, 9$ are 103.584, 174.998, 464.956, and 864.991, respectively. These are Monte Carlo 0.95 quantiles of the corresponding Brownian-bridge quadratic-form limits, computed with 200000 Brownian paths and 1000 grid points.

Tree \mathbf{b}_{HG}	node counts (N_ℓ^{HG})	weights (w_ℓ^{HG})
[4, 4]	1, 4, 16	0.0476, 0.1905, 0.7619
[4, 8]	1, 4, 32	0.0270, 0.1081, 0.8649
[4, 4, 4]	1, 4, 16, 64	0.0118, 0.0471, 0.1882, 0.7529

Table 11: HiGrad public tree budget at $n = 3 \times 10^8$. Here N_ℓ^{HG} is the number of nodes at level ℓ , and w_ℓ^{HG} is the fraction of users assigned to that level. In each row, the displayed weights sum to one up to rounding.

B Additional Numerical Summaries

This appendix reports supplementary point-estimation and $n = 3 \times 10^8$ coverage summaries for the decoded estimating-equation experiments. Table 12 expands the sample-size trajectories behind the root- n

diagnostic in the main text. Tables 13, 14, and 15 give alternative aggregations of the estimation-only direct Laplace and face-exponential comparisons. Tables 16–20 summarize inference behavior in difficult cells and across the final-horizon grid. A single 500-replication coverage estimate has Monte Carlo standard error at most 0.023.

n	(0.5, 2, 2)	(0.75, 8, 0.5)	(0.75, 8, 16)	(0.75, 8, ∞)
10^3	6.07×10^{-1}	9.90×10^{-1}	7.06×10^{-1}	7.02×10^{-1}
3×10^3	3.20×10^{-1}	9.86×10^{-1}	4.26×10^{-1}	4.20×10^{-1}
10^4	1.25×10^{-1}	9.53×10^{-1}	1.63×10^{-1}	1.59×10^{-1}
3×10^4	5.89×10^{-2}	8.72×10^{-1}	6.34×10^{-2}	6.06×10^{-2}
10^5	3.04×10^{-2}	6.87×10^{-1}	2.56×10^{-2}	2.35×10^{-2}
3×10^5	1.71×10^{-2}	4.62×10^{-1}	1.29×10^{-2}	1.15×10^{-2}
10^6	9.26×10^{-3}	2.46×10^{-1}	6.67×10^{-3}	5.96×10^{-3}
3×10^6	5.28×10^{-3}	1.33×10^{-1}	3.70×10^{-3}	3.29×10^{-3}
10^7	2.81×10^{-3}	6.70×10^{-2}	2.01×10^{-3}	1.78×10^{-3}
3×10^7	1.62×10^{-3}	3.86×10^{-2}	1.17×10^{-3}	1.04×10^{-3}
10^8	8.98×10^{-4}	2.07×10^{-2}	6.31×10^{-4}	5.63×10^{-4}
3×10^8	5.25×10^{-4}	1.17×10^{-2}	3.69×10^{-4}	3.29×10^{-4}

Table 12: Mean Euclidean estimation error at reported sample sizes $n \in \{1, 3\} \times 10^{r_n}$, $r_n = 3, \dots, 8$. The columns fix $(\tau, p, \varepsilon) = (0.5, 2, 2)$, $(0.75, 8, 0.5)$, $(0.75, 8, 16)$, and the nonprivate ASGD reference $(0.75, 8, \infty)$. This table expands the trajectory information summarized in the main-text effective-information diagnostic. Each mean is computed over 500 independent Monte Carlo replications.

ε	Direct Laplace	Face-exponential
0.5	2.58	$4.43 \times 10^{2 \times}$
1	2.56	$8.20 \times 10^{2 \times}$
2	2.48	$1.94 \times 10^{3 \times}$
4	2.36	$3.49 \times 10^{3 \times}$
8	2.28	$4.97 \times 10^{2 \times}$
16	1.59	15.9

Table 13: Median final-horizon estimation-error ratio by privacy budget for the geometric baselines. Each entry is the median, over $\tau \in \{0.5, 0.75\}$ and $p \in \{1, 2, 5, 8\}$, of the baseline mean Euclidean error divided by the corresponding $\text{CQ}_X(q, s)$ mean Euclidean error at $n = 3 \times 10^8$. A superscript \times marks a face-exponential aggregate dominated by cells whose reported errors are governed by projection-boundary saturation.

p	Direct Laplace	Face-exponential
1	1.54	36.2 [×]
2	1.84	22.5 [×]
5	3.02	22.6 [×]
8	3.81	17.8 [×]

Table 14: Median final-horizon estimation-error ratio by dimension for the geometric baselines. Each entry is the median, over $\tau \in \{0.5, 0.75\}$ and $\varepsilon \in \{0.5, 1, 2, 4, 8, 16\}$, of the baseline mean Euclidean error divided by the corresponding $\text{CQ}_X(q, s)$ mean Euclidean error at $n = 3 \times 10^8$. A superscript \times marks a face-exponential aggregate dominated by cells whose reported errors are governed by projection-boundary saturation.

Baseline	$Q_{0.25}$	median	$Q_{0.75}$	median MCSE	largest-ratio cell
Direct Laplace	1.76	2.31	3.37	0.078	(0.75, 8, 4): 4.19
Face-exponential	4.65	17.8 [×]	$4.01 \times 10^{3 \times}$	0.261	(0.75, 2, 4) [×] : 3.46×10^4

Table 15: Distribution of final-horizon estimation-error ratios for the geometric baselines over the 48 private finite- ε cells. Ratios compare each baseline mean Euclidean error with the $\text{CQ}_X(q, s)$ mean in the same (τ, p, ε) cell. The MCSE column is the median delta-method Monte Carlo standard error of the ratio, using 200 baseline replications and 500 $\text{CQ}_X(q, s)$ replications. A superscript \times marks a face-exponential aggregate or cell whose reported error is governed by projection-boundary saturation.

ε	SN			DC			HiGrad [4, 4]		
	coord. 0	dense	ell.	coord. 0	dense	ell.	coord. 0	dense	ell.
0.5	0.900	0.934	0.586	0.006	0.942	0.684	0.648	0.868	0.746
1	0.916	0.938	0.714	0.020	0.944	0.724	0.668	0.904	0.870
2	0.946	0.954	0.840	0.492	0.950	0.904	0.878	0.938	0.920
4	0.928	0.946	0.866	0.854	0.944	0.944	0.916	0.938	0.934
8	0.946	0.960	0.916	0.744	0.946	0.928	0.922	0.956	0.944
16	0.956	0.954	0.932	0.848	0.952	0.946	0.936	0.924	0.938
∞	0.956	0.950	0.904	0.886	0.944	0.942	0.930	0.944	0.938

Table 16: Coverage sensitivity at $n = 3 \times 10^8$ in the upper-quantile larger- p design $(\tau, p) = (0.75, 8)$. Finite- ε rows vary ε ; the ∞ row is the nonprivate ASGD reference. The HiGrad columns use only the public tree $\mathbf{b}_{\text{HG}} = [4, 4]$; Table 17 isolates tree sensitivity. Coordinate entries refer to coordinate 0, dense denotes the $a_{\text{den}} = d^{-1/2} \mathbf{1}_d$ contrast, and ellipsoid denotes full-coefficient coverage. Each displayed coverage estimate is based on 500 independent Monte Carlo replications.

(τ, p, ε)	Estimand	$\mathbf{b}_{\text{HG}} = [4, 4]$	$\mathbf{b}_{\text{HG}} = [4, 8]$	$\mathbf{b}_{\text{HG}} = [4, 4, 4]$
(0.50, 2, 2)	coord. 0	0.950	0.952	0.934
(0.50, 2, 2)	dense	0.956	0.954	0.936
(0.50, 2, 2)	ellipsoid	0.952	0.952	0.934
(0.75, 2, 2)	coord. 0	0.932	0.916	0.904
(0.75, 2, 2)	dense	0.934	0.918	0.926
(0.75, 2, 2)	ellipsoid	0.920	0.914	0.896
(0.75, 8, 0.5)	coord. 0	0.648	0.498	0.176
(0.75, 8, 0.5)	dense	0.868	0.734	0.748
(0.75, 8, 0.5)	ellipsoid	0.746	0.316	0.136
(0.75, 8, 16)	coord. 0	0.936	0.932	0.914
(0.75, 8, 16)	dense	0.924	0.940	0.938
(0.75, 8, 16)	ellipsoid	0.938	0.918	0.920

Table 17: HiGrad empirical 95% coverage at $n = 3 \times 10^8$ and fixed design points, varying only the public tree. Coordinate rows report coordinate 0, dense denotes the $a_{\text{den}} = d^{-1/2} \mathbf{1}_d$ contrast, and ellipsoid denotes full-coefficient coverage. For HiGrad, \mathbf{b}_{HG} denotes the public branching vector; $\mathbf{b}_{\text{HG}} = [4, 4]$, $\mathbf{b}_{\text{HG}} = [4, 8]$, and $\mathbf{b}_{\text{HG}} = [4, 4, 4]$ have $R_{\text{HG}} = 16$, 32, and 64 leaves, respectively. Each displayed coverage estimate is based on 500 independent Monte Carlo replications.

(τ, p, ε)	Method	coord. 0		dense		ellipsoid	
		cov.	mean length	cov.	mean length	cov.	mean volume
(0.50, 2, 2)	SN	0.946	6.48×10^{-4}	0.940	1.65×10^{-3}	0.934	5.74×10^{-9}
	DC	0.948	6.09×10^{-4}	0.950	1.59×10^{-3}	0.954	8.98×10^{-9}
	HiGrad [4, 4]	0.950	5.59×10^{-4}	0.956	1.39×10^{-3}	0.952	3.00×10^{-9}
	HiGrad [4, 8]	0.952	5.37×10^{-4}	0.954	1.34×10^{-3}	0.952	2.30×10^{-9}
	HiGrad [4, 4, 4]	0.934	5.21×10^{-4}	0.936	1.30×10^{-3}	0.934	1.99×10^{-9}
(0.75, 8, 0.5)	SN	0.900	5.28×10^{-3}	0.934	1.91×10^{-2}	0.586	1.03×10^{-15}
	DC	0.006	4.14×10^{-3}	0.942	1.78×10^{-2}	0.684	3.88×10^{-13}
	HiGrad [4, 4]	0.648	3.78×10^{-3}	0.868	1.50×10^{-2}	0.746	4.22×10^{-15}
	HiGrad [4, 8]	0.498	3.63×10^{-3}	0.734	1.40×10^{-2}	0.316	1.32×10^{-16}
	HiGrad [4, 4, 4]	0.176	3.51×10^{-3}	0.748	1.29×10^{-2}	0.136	3.13×10^{-17}

Table 18: Final-horizon interval and ellipsoid size for two representative cells at $n = 3 \times 10^8$. Coordinate and dense columns report empirical coverage and mean interval length. Ellipsoid columns report empirical coverage and mean ellipsoid volume. The first cell is the moderate $p = 2, \varepsilon = 2$ design used in main-text Table 7; the second is the upper-quantile, larger- p , small- ε design discussed in Section 4. Each entry is computed from 500 independent Monte Carlo replications.

ε	Method	coordinate	dense	ellipsoid
0.5	SN	0.933 [0.900, 0.966]	0.934 [0.912, 0.960]	0.851 [0.586, 0.956]
	DC	0.904 [0.006, 0.974]	0.950 [0.938, 0.964]	0.895 [0.684, 0.962]
1	SN	0.940 [0.916, 0.970]	0.950 [0.938, 0.968]	0.894 [0.714, 0.958]
	DC	0.913 [0.020, 0.974]	0.948 [0.942, 0.956]	0.911 [0.724, 0.950]
2	SN	0.943 [0.916, 0.960]	0.946 [0.928, 0.962]	0.918 [0.840, 0.954]
	DC	0.931 [0.492, 0.966]	0.949 [0.926, 0.972]	0.936 [0.904, 0.954]
4	SN	0.948 [0.928, 0.974]	0.952 [0.946, 0.958]	0.935 [0.866, 0.960]
	DC	0.944 [0.854, 0.966]	0.949 [0.930, 0.958]	0.948 [0.934, 0.960]
8	SN	0.948 [0.920, 0.970]	0.953 [0.934, 0.962]	0.941 [0.916, 0.968]
	DC	0.942 [0.744, 0.964]	0.946 [0.934, 0.956]	0.944 [0.928, 0.972]
16	SN	0.948 [0.918, 0.974]	0.951 [0.942, 0.962]	0.946 [0.928, 0.964]
	DC	0.941 [0.848, 0.964]	0.945 [0.932, 0.952]	0.946 [0.936, 0.958]
∞	SN	0.948 [0.916, 0.978]	0.950 [0.938, 0.964]	0.940 [0.904, 0.956]
	DC	0.942 [0.886, 0.966]	0.945 [0.930, 0.962]	0.944 [0.930, 0.954]

Table 19: Final 95% coverage at $n = 3 \times 10^8$ for SN and DC by privacy budget and estimand. Entries are mean empirical coverage with [min, max] over the cells at the displayed ε , method, and estimand. For each ε -method row, the coordinate entry summarizes 40 coordinate-specific coverages over $\tau \in \{0.5, 0.75\}$, $p \in \{1, 2, 5, 8\}$, and coordinates; the dense and ellipsoid entries summarize 8 cell-level coverages. Dense denotes the $a_{\text{den}} = d^{-1/2}\mathbf{1}_d$ contrast, and ellipsoid denotes full-coefficient coverage. The $\varepsilon = \infty$ rows use the nonprivate ASGD reference. Each underlying coverage estimate is computed from 500 independent replications. HiGrad summaries are reported separately by tree in Table 20.

ε	Tree	R_{HG}	coordinate	dense	ellipsoid
0.5	[4, 4]	16	0.902 [0.648, 0.962]	0.922 [0.868, 0.948]	0.895 [0.746, 0.948]
	[4, 8]	32	0.848 [0.498, 0.960]	0.875 [0.734, 0.922]	0.754 [0.316, 0.920]
	[4, 4, 4]	64	0.829 [0.176, 0.962]	0.876 [0.748, 0.932]	0.704 [0.136, 0.944]
1	[4, 4]	16	0.924 [0.668, 0.958]	0.937 [0.904, 0.954]	0.919 [0.866, 0.964]
	[4, 8]	32	0.887 [0.478, 0.950]	0.910 [0.874, 0.940]	0.840 [0.578, 0.942]
	[4, 4, 4]	64	0.876 [0.238, 0.962]	0.910 [0.842, 0.944]	0.797 [0.342, 0.956]
2	[4, 4]	16	0.937 [0.878, 0.958]	0.941 [0.908, 0.966]	0.934 [0.912, 0.954]
	[4, 8]	32	0.920 [0.808, 0.958]	0.926 [0.890, 0.954]	0.907 [0.804, 0.952]
	[4, 4, 4]	64	0.914 [0.748, 0.964]	0.924 [0.906, 0.940]	0.881 [0.720, 0.954]
4	[4, 4]	16	0.944 [0.888, 0.970]	0.951 [0.938, 0.966]	0.947 [0.932, 0.976]
	[4, 8]	32	0.931 [0.876, 0.966]	0.939 [0.900, 0.976]	0.921 [0.848, 0.948]
	[4, 4, 4]	64	0.930 [0.882, 0.958]	0.931 [0.908, 0.946]	0.905 [0.818, 0.934]
8	[4, 4]	16	0.942 [0.916, 0.960]	0.948 [0.936, 0.958]	0.940 [0.930, 0.950]
	[4, 8]	32	0.941 [0.916, 0.968]	0.944 [0.898, 0.978]	0.935 [0.912, 0.968]
	[4, 4, 4]	64	0.938 [0.882, 0.960]	0.942 [0.926, 0.954]	0.927 [0.884, 0.950]
16	[4, 4]	16	0.948 [0.926, 0.970]	0.948 [0.924, 0.964]	0.947 [0.938, 0.960]
	[4, 8]	32	0.946 [0.926, 0.964]	0.946 [0.916, 0.966]	0.939 [0.918, 0.954]
	[4, 4, 4]	64	0.945 [0.914, 0.968]	0.942 [0.934, 0.960]	0.942 [0.920, 0.962]
∞	[4, 4]	16	0.945 [0.922, 0.974]	0.943 [0.928, 0.960]	0.941 [0.922, 0.952]
	[4, 8]	32	0.944 [0.920, 0.968]	0.942 [0.918, 0.952]	0.942 [0.912, 0.956]
	[4, 4, 4]	64	0.939 [0.900, 0.960]	0.942 [0.930, 0.950]	0.929 [0.906, 0.950]

Table 20: HiGrad final 95% coverage by privacy budget and tree at $n = 3 \times 10^8$. Entries are mean empirical coverage with [min, max] over the cells at the displayed ε , tree, and estimand. For each ε -tree row, the coordinate entry summarizes 40 coordinate-specific coverages over $\tau \in \{0.5, 0.75\}$, $p \in \{1, 2, 5, 8\}$, and coordinates; the dense and ellipsoid entries summarize 8 cell-level coverages. Dense denotes the $a_{\text{den}} = d^{-1/2} \mathbf{1}_d$ contrast, and ellipsoid denotes full-coefficient coverage. The $\varepsilon = \infty$ rows use the nonprivate ASGD reference. Each underlying coverage estimate is computed from 500 independent replications.

References

- A. Aamand, L. Boninsegna, M. Gentle, J. Imola, and R. Pagh. Lightweight protocols for distributed private quantile estimation. In *Proceedings of ICML*, volume 267 of *Proceedings of Machine Learning Research*, pages 27–58, 2025.
- J. Acharya, Z. Sun, and H. Zhang. Hadamard response: Estimating distributions privately, efficiently, and with little communication. In *Proceedings of AISTATS*, volume 89 of *Proceedings of Machine Learning Research*, pages 1120–1129, 2019.
- D. Alabi, O. Ben-Eliezer, and A. Chaturvedi. Bounded space differentially private quantiles. *Transactions on Machine Learning Research*, 2023.
- D. Alistarh, D. Grubic, J. Li, R. Tomioka, and M. Vojnovic. QSGD: Communication-efficient SGD via gradient quantization and encoding. In *Advances in Neural Information Processing Systems*, volume 30, 2017.
- J. Angrist, V. Chernozhukov, and I. Fernández-Val. Quantile regression under misspecification, with an application to the U.S. wage structure. *Econometrica*, 74(2):539–563, 2006.
- H. Asi, V. Feldman, and K. Talwar. Optimal algorithms for mean estimation under local differential privacy. In *Proceedings of ICML*, volume 162 of *Proceedings of Machine Learning Research*, pages 1046–1056, 2022.
- H. Asi, V. Feldman, J. Nelson, H. L. Nguyen, and K. Talwar. Fast optimal locally private mean estimation via random projections. *Advances in Neural Information Processing Systems*, 2023.
- F. Bach and E. Moulines. Non-asymptotic analysis of stochastic approximation algorithms for machine learning. *Advances in Neural Information Processing Systems*, 2011.
- M. Banerjee, C. Durot, and B. Sen. Divide and conquer in nonstandard problems and the super-efficiency phenomenon. *Annals of Statistics*, 47(2):720–757, 2019.
- R. Bassily and A. Smith. Local, private, efficient protocols for succinct histograms. In *Proceedings of STOC*, pages 127–135, 2015.
- L. Bottou, F. E. Curtis, and J. Nocedal. Optimization methods for large-scale machine learning. *SIAM Review*, 60(2):223–311, 2018.
- L. Cai, Q. Hu, J. Sun, and S. Wu. Time-uniform and asymptotic confidence sequence of quantile under local differential privacy. *Advances in Neural Information Processing Systems*, 38:114488–114520, 2025.

- L. Cai, Q. Hu, and S. Wu. Federated learning of quantile inference under local differential privacy. In *International Conference on Learning Representations*, 2026a.
- L. Cai, Q. Hu, and S. Wu. Privacy-aware data integration for enhanced quantile inference under heterogeneity. In *Forty-third International Conference on Machine Learning*, 2026b.
- C. L. Canonne and M. Gentle. Locally private histograms in all privacy regimes. In *Leibniz International Proceedings in Informatics*, volume 325 of *LIPICs*, pages 25:1–25:24, 2025.
- D. Chen and G. A. Chua. Differentially private stochastic convex optimization under a quantile loss function. In *Proceedings of ICML*, volume 202 of *Proceedings of Machine Learning Research*, pages 4435–4461, 2023.
- X. Chen, J. D. Lee, X. T. Tong, and Y. Zhang. Statistical inference for model parameters in stochastic gradient descent. *The Annals of Statistics*, 48(1):251–273, 2020.
- V. Chernozhukov and I. Fernández-Val. Inference for extremal conditional quantile models, with an application to market and birthweight risks. *The Review of Economic Studies*, 78(2):559–589, 2011.
- G. Cormode, T. Kulkarni, and D. Srivastava. Answering range queries under local differential privacy. *Proceedings of the VLDB Endowment*, 12(10):1126–1138, 2019.
- H. Dette and C. Graw. Uncertainty quantification by block bootstrap for differentially private stochastic gradient descent. *arXiv preprint arXiv:2405.12553*, 2024.
- J. C. Duchi, M. I. Jordan, and M. J. Wainwright. Local privacy and statistical minimax rates. In *Proceedings of FOCS*, pages 429–438, 2013.
- J. C. Duchi, M. I. Jordan, and M. J. Wainwright. Minimax optimal procedures for locally private estimation. *Journal of the American Statistical Association*, 113(521):182–215, 2018.
- D. Durfee. Unbounded differentially private quantile and maximum estimation. In *Advances in Neural Information Processing Systems*, volume 36, 2023.
- C. Dwork and J. Lei. Differential privacy and robust statistics. In *Proceedings of STOC*, pages 371–380, 2009.
- C. Dwork and A. Roth. The algorithmic foundations of differential privacy. *Foundations and Trends in Theoretical Computer Science*, 9(3–4):211–407, 2014.
- C. Dwork, F. McSherry, K. Nissim, and A. Smith. Calibrating noise to sensitivity in private data analysis. In *Theory of Cryptography Conference*, pages 265–284, 2006.

- U. Erlingsson, V. Pihur, and A. Korolova. RAPPOR: Randomized aggregatable privacy-preserving ordinal response. In *Proceedings of ACM CCS*, pages 1054–1067, 2014.
- Y. Fang, J. Xu, and L. Yang. Online bootstrap confidence intervals for the stochastic gradient descent estimator. *Journal of Machine Learning Research*, 19(78):1–21, 2018.
- M. Gaboardi, R. Rogers, and O. Sheffet. Locally private mean estimation: z -test and tight confidence intervals. In *Proceedings of AISTATS*, volume 89 of *Proceedings of Machine Learning Research*, pages 2545–2554, 2019.
- S. Gadat and F. Panloup. Optimal non-asymptotic analysis of the Ruppert–Polyak averaging stochastic algorithm. *Stochastic Processes and their Applications*, 156:312–348, 2023.
- J. Gillenwater, M. Joseph, and A. Kulesza. Differentially private quantiles. In *Proceedings of ICML*, volume 139 of *Proceedings of Machine Learning Research*, pages 3713–3722, 2021.
- S. Gupta, A. Agrawal, K. Gopalakrishnan, and P. Narayanan. Deep learning with limited numerical precision. *arXiv preprint arXiv:1502.02551*, 2015.
- P. Hall and C. C. Heyde. *Martingale Limit Theory and Its Application*. Academic Press, 1980.
- Q. Hu and Y. Liu. Censoring with plausible deniability: Asymmetric local privacy for multi-category cdf estimation. In *Forty-third International Conference on Machine Learning*, 2026.
- J. Imola, F. Boninsegna, H. Keller, A. Aamand, A. Roy Chowdhury, and R. Pagh. Differentially private quantiles with smaller error. *arXiv preprint arXiv:2505.13662*, 2025.
- P. Kairouz, S. Oh, and P. Viswanath. Extremal mechanisms for local differential privacy. *Journal of Machine Learning Research*, 17(17):1–51, 2016.
- H. Kaplan, S. Schnapp, and U. Stemmer. Differentially private approximate quantiles. In *Proceedings of ICML*, volume 162 of *Proceedings of Machine Learning Research*, pages 10751–10761, 2022.
- R. Koenker. *Quantile Regression*. Cambridge University Press, 2005.
- R. Koenker and G. Bassett. Regression quantiles. *Econometrica*, 46(1):33–50, 1978.
- H. J. Kushner and G. G. Yin. *Stochastic Approximation and Recursive Algorithms and Applications*. Springer, second edition, 2003.
- C. Lallanne, A. Garivier, and R. Gribonval. Private statistical estimation of many quantiles. In *Proceedings of ICML*, volume 202 of *Proceedings of Machine Learning Research*, pages 18399–18418, 2023.

- S. Lee, Y. Liao, M. H. Seo, and Y. Shin. Fast and robust online inference with stochastic gradient descent via random scaling. *Proceedings of the AAAI Conference on Artificial Intelligence*, 36(7):7381–7389, 2022.
- Z. Li, T. Wang, M. Lopuhaä-Zwakenberg, B. Skoric, and N. Li. Estimating numerical distributions under local differential privacy. In *Proceedings of ACM SIGMOD*, pages 621–635, 2020.
- Y. Liu, Q. Hu, L. Ding, B. Jiang, and L. Kong. Online local differential private quantile inference via self-normalization. In *Proceedings of ICML*, volume 202 of *Proceedings of Machine Learning Research*, pages 21698–21714, 2023.
- Y. Liu, Q. Hu, and L. Kong. Tuning-free estimation and inference of CDF under local differential privacy. In *Proceedings of ICML*, volume 235 of *Proceedings of Machine Learning Research*, pages 31147–31164, 2024.
- Q. Lu, S. X. Chen, and Y. Qiu. Versatile differentially private learning for general loss functions. *The Annals of Statistics*, 54(2):692–717, 2026.
- New York City Taxi and Limousine Commission. TLC Trip Record Data: Yellow Taxi Trip Records, January 2024, 2024.
- K. Nissim, S. Raskhodnikova, and A. Smith. Smooth sensitivity and sampling in private data analysis. In *Proceedings of STOC*, pages 75–84, 2007.
- H. Ono, K. Minami, and H. Hino. One-bit submission for locally private quasi-MLE: Its asymptotic normality and limitation. In *Proceedings of AISTATS*, volume 151 of *Proceedings of Machine Learning Research*, pages 2762–2783, 2022.
- A. Pastore and M. Gastpar. Locally differentially-private randomized response for discrete distribution learning. *Journal of Machine Learning Research*, 22:1–56, 2021.
- B. T. Polyak and A. B. Juditsky. Acceleration of stochastic approximation by averaging. *SIAM Journal on Control and Optimization*, 30(4):838–855, 1992.
- H. Robbins and D. Siegmund. A convergence theorem for nonnegative almost supermartingales and some applications. In *Optimizing Methods in Statistics*, pages 233–257. Academic Press, 1971.
- D. Ruppert. Efficient estimations from a slowly convergent Robbins–Monro process. Technical report, Cornell University, 1988.
- X. Shao. A self-normalized approach to confidence interval construction in time series. *Journal of the Royal Statistical Society: Series B*, 72(3):343–366, 2010.

- X. Shao. Self-normalization for time series: A review of recent developments. *Journal of the American Statistical Association*, 110(512):1797–1817, 2015.
- Y. Shen, D. Xia, and W.-X. Zhou. Online quantile regression. *Journal of Machine Learning Research*, 26(231):1–55, 2025a.
- Z. Shen, C. Wang, S. Wang, and Y. Yan. High-dimensional differentially private quantile regression: Distributed estimation and statistical inference. *arXiv preprint arXiv:2508.05212*, 2025b.
- A. Smith. Privacy-preserving statistical estimation with optimal convergence rates. In *Proceedings of STOC*, pages 813–821, 2011.
- W. J. Su and Y. Zhu. HiGrad: Uncertainty quantification for online learning and stochastic approximation. *Journal of Machine Learning Research*, 24:1–53, 2023.
- K. M. Tan, H. Battey, and W.-X. Zhou. Communication-constrained distributed quantile regression with optimal statistical guarantees. *Journal of Machine Learning Research*, 23:1–61, 2022.
- T. Tran, M. Reimherr, and A. Slavkovic. Differentially private quantile regression. In *Privacy in Statistical Databases*, volume 14915 of *Lecture Notes in Computer Science*, pages 18–34. Springer, 2024.
- D. Wang, M. Gaboardi, A. Smith, and J. Xu. Empirical risk minimization in the non-interactive local model of differential privacy. *Journal of Machine Learning Research*, 21:1–39, 2020.
- D. Wang, L. Hu, H. Zhang, M. Gaboardi, and J. Xu. Generalized linear models in non-interactive local differential privacy with public data. *Journal of Machine Learning Research*, 24:1–57, 2023.
- N. Wang, X. Xiao, Y. Yang, J. Zhao, S. C. Hui, H. Shin, J. Shin, and G. Yu. Collecting and analyzing multidimensional data with local differential privacy. In *Proceedings of ICDE*, pages 638–649, 2019.
- Z. Wang, G. Cheng, and J. Awan. Differentially private bootstrap: New privacy analysis and inference strategies. *Journal of Machine Learning Research*, 26:1–57, 2025.
- S. L. Warner. Randomized response: A survey technique for eliminating evasive answer bias. *Journal of the American Statistical Association*, 60(309):63–69, 1965.
- J. Xie, E. Shi, B. Jiang, L. Kong, and X. He. Online differentially private inference in stochastic gradient descent. *arXiv preprint arXiv:2505.08227*, 2025.
- M. Ye and A. Barg. Optimal schemes for discrete distribution estimation under locally differential privacy. *IEEE Transactions on Information Theory*, 64(8):5662–5676, 2018.
- Y. Zhu and J. Dong. On constructing confidence region for model parameters in stochastic gradient descent via batch means. In *Proceedings of the Winter Simulation Conference*, pages 1–12, 2021.